UU-76-2-Z

DEPARTMENT OF GEOLOGY AND GEOPHYSICS

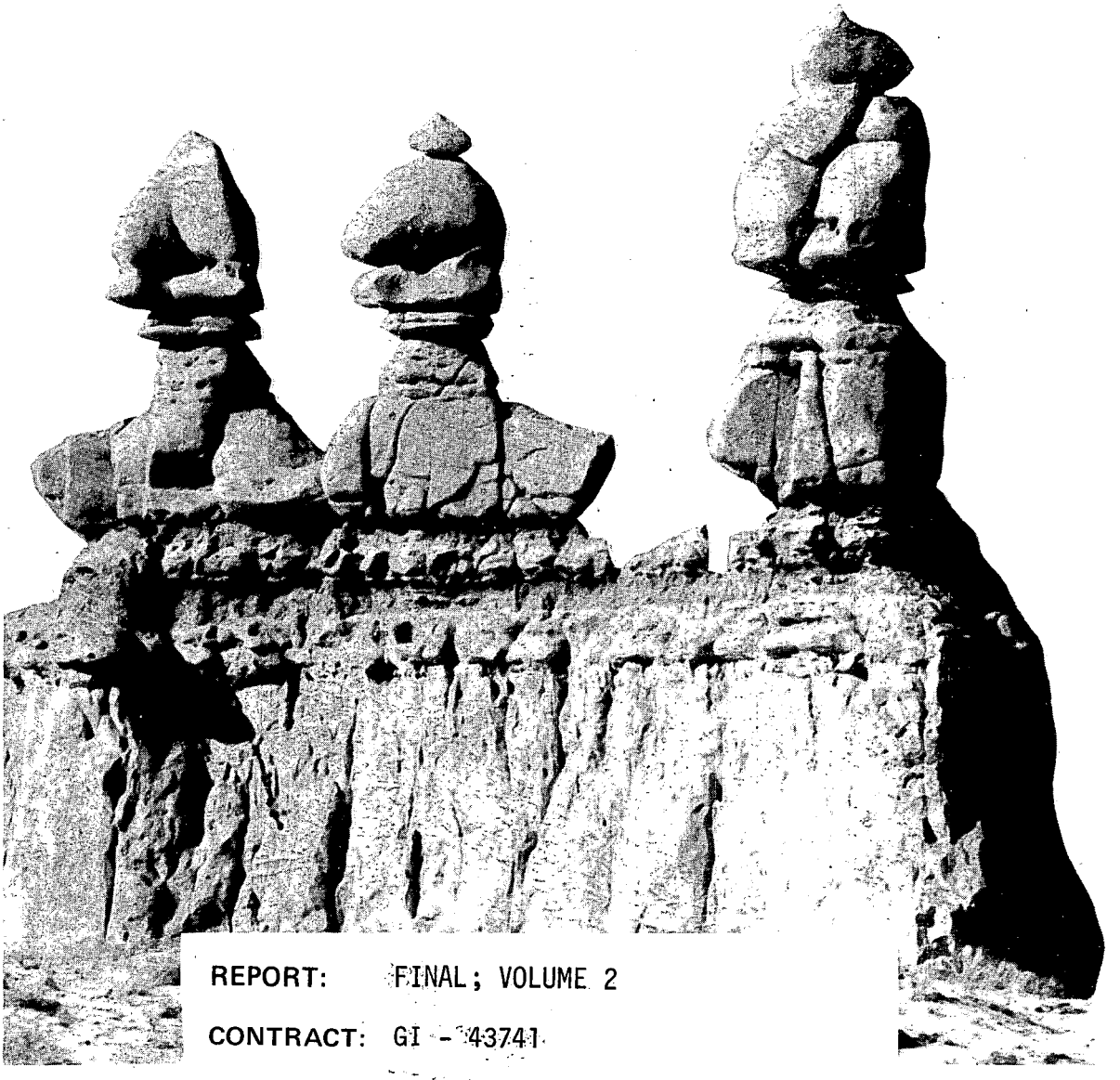

REPORT: FINAL; VOLUME 2

CONTRACT: GI - 43741

AGENCY: NATIONAL SCIENCE FOUNDATION

TITLE: DIPOLE-DIPOLE RESISTIVITY SURVEYS, ROOSEVELT HOT SPRINGS KGRA

AUTHORS: S. H. Ward, W. R. Sill

JUN 1976

UNIVERSITY OF UTAH SALT LAKE CITY, UTAH 84112

DISCLAIMER

FINAL REPORT; VOLUME 2

Dipole-Dipole Resistivity Surveys, Roosevelt Hot Springs KGRA

National Science Foundation
Grant GI-43741

S. H. Ward
and
W. R. Sill

Table of Contents

1.0 Introduction 1

2.0 Data Presentation 2

3.0 Interpretation 3

3.2 Quantitative 12

4.0 Comparison of bipole-dipole and dipole-dipole resistivity Techniques 20

5.0 Conclusions 21

6.0 Recommendations 23

7.0 Acknowledgements 24

References 25

List of Illustrations 27

ABSTRACT

Dipole-dipole resistivity surveys using 100m, 300m and 1 km dipoles at Roosevelt Hot Springs KGRA, near Milford, Utah, have been interpreted qualitatively and quantitatively.

The qualitative interpretation draws attention to three dense fracture sets in the vicinity of wells proven to be capable of stream production. Coincident hydrothermal alteration and brines in fractures produce pronounced resistivity lows in the vicinities of productive steam wells. East-west and a northwest-southeast fracture sets seem to carry fresh water into and brine away from the center of a convective hydrothermal system. Pore porosities of order 20% seem probable for rocks to depths of order 500m. Fracture porosity is to be added. No heat source has been detected but this is not unreasonable considering a maximum depth of exploration of 1.5 km for the dipole-dipole survey used.

A two-dimensional transmission-surface forward algorithm permitted us to model the observed data. From the two-dimensional models we conclude that a) the north-south fractures are conductive at least to depths of order 500m, but lack of resolution of the resistivity data prohibits us from commenting on conductive fractures at greater depths, b) the low resistivities of the fractures are attributed either to clay and pyrite alteration or to hot brine in the fractures or to both, c) the marked increase in resistivity at about 500m is attributed either to a reduction in alteration (likely), to the replacement of brine by steam, or to tightening of the fractures, or to lack of resolution of the resistivity method (likely).

Report on Dipole-Dipole Resistivity Surveys,

Roosevelt Hot Springs KGRA

Introduction

During the summers of 1974 and 1975, dipole-dipole resistivity surveys were conducted at Roosevelt Hot Springs KGRA. Three different dipole spacings were used; 99km of traverse line were surveyed with 100m dipoles, 50km with 300m dipoles, and 44km with 1km dipoles. Three different degrees of resolution and depth of exploration were thereby achieved. For 100m, 300m and 1km dipoles, the frequencies employed were 1.0hz, 0.3hz, and 0.1hz, respectively. Electromagnetic coupling was thereby kept below measuring error.

The objectives of the resistivity surveying were to detect and delineate regions of low resistivity associated with fracturing, brines, high temperatures, and clay alteration. The resistivity of rocks that are typical of hydrothermal environments is due to two main conduction mechanisms. The mechanisms are electrolytic conduction through pores and fractures and surface conduction due to a thin zone of cations attracted to those mineral surfaces with net negative charges (especially clay minerals). For saturated rocks, the resistivity due to electrolytic conduction is a function of the effective porosity of the fractured rock, of the temperature, and of the salinity of the fluid filling the pores and fractures. The resistivity decreases as the effective porosity, water saturation, salinity, and temperature increase. The presence of clay minerals and pyrite will also decrease the resistivity. A reasonably complete discussion of these conduction mechanisms is given by Ward & Fraser (1967).

The locations of traverse lines used for the 100m dipole surveys are shown in Figure 43. The locations of lines used for the 300m dipole surveys are shown in Figure 45. Three traverses were performed with 1km dipoles

and their locations are shown in Figure 46. These latter traverses have labels such as W7 or 13E on their ends; these labels indicated distances in kilometers. Elsewhere, distances are measured in meters or hundreds of meters. The general location of the grid for the 100m and 300m dipole surveys is also shown in this latter figure.

2.0 Data Presentation

The apparent resistivities have been plotted in psuedo-sections in Figures 1 through 41. [Figures 1 through 38 will be made available upon special request but are deleted from the body of this report in order to reduce bulk and cost]. Each data point in the pseudo section is plotted at the intersection of two lines drawn at 45° from the centers of the transmitting and receiving dipoles as shown in Figure 42. In this latter figure, a is the dipole length and n is the separation which assumes the discrete values n = 1,2,3,4,---. This is the standard method of presenting data from a dipole-dipole resistivity survey. The larger the separation the deeper the exploration so that each of Figures 1 through 41 represents combined profiling - sounding.

For dipole lengths of 100m, 300m and 1km, the scales at which the pseudo-sections have been plotted are 1:5000, 1:15000, and 1:50000, respectively.

We have departed from convention in drawing solid and dashed bars over regions of resistivity < 10 Ωm and 10 to 20 Ωm, respectively. This procedure merely draws attention to zones of low resistivity and does not imply any qualitative interpretation.

The 100m first separation (n=1) apparent resistivity values have been contoured in Fig. 44 while the 300m first separation values have been contoured in Figure 45; both plan maps are on a scale of 1:24000 and may be overlain on the 7 1/2 minute topographic quadrangles of the region.

3.0 Interpretation

3.1 Qualitative

3.1.1 Fractures

The first-separation apparent resistivity contour maps of Figures 44 and 45 were used with the pseudo-sections of Figures 1 through 41, the aeromagnetic map of the area, airphotos plus mapped and interpreted geology to produce the fracture map of Figure 47. This map is at scale of 1:24000 and plotted thereon is sufficient information about the grid, the sections and latitudes to permit ready correlation with the 7 1/2 minute topographic quadrangles of the area.

Three dominant fracture sets are observed: a north-south set, an east-west set, and a northwest-southeast set.

The region between the Dome Fault and Fault 1 appears to be a continuous fracture zone. Faults 2 and 4 appear to be downthrown to the south according to the distribution of resistivity values seen in Figures 26 and 28 through 31. Peterson and Whelan (1975) interpret Dome Fault to be upthrown to the west. Elsewhere (Ward, 1976) the aeromagnetic data has been interpreted to indicate a right-lateral offset of 1 km on Negro Mag Fault. No other fault motions are known.

The locations of seven wells, drilled to evaluate the geothermal resource potential, are shown in Figure 47. Each well was drilled through highly fractured ground. Wells OH-1 and 82-33 reportedly are "dry", hole 9-1 did not encounter highly fractured ground, while holes 13-10, 3-1 and 54-3 are "capable of commercial production." Hole 12-35 is still being tested. Evidently all holes west of the Dome Fault are "dry". Observation of outcrop and drill core which we obtained from shallow drill holes DDH1A and DDH1B, coupled with interpretation of aeromagnetic data (Ward, 1976), lead us to believe that the west side of the Dome Fault between 1000N and 5500N, is underlain mostly by Precambrian rocks;

the width of the sub-outcropping Precambrian is at least 1 km.

3.1.2 Alteration

Holes DDH1A and DDH1B intersected altered alluvium and altered Precambrian to depths of 217 feet (66m) and 231 feet (71m), respectively. The following alteration products were encountered in hole DDH1A (Parry, 1976)

Depth	Alteration Product	
20' - 60' (6m-18m)	Alunite	alluvium
60' - 85' (18m-26m)	Alunite, kaolinite	alluvium
85' - 106' (26m-32m)	Alunite ± kaolinite	alluvium
WATER TABLE, @ 115' (35m)		
105' - 185' (32m-56m)	Montmorillonite, kaolinite, Kmica + 2% py	Precambrian granite gneiss
185' - 217' (56m-66m)	Montmorillonite, kaolinite, Kmica + 4% py	Precambrian granite gneiss

The depth to which these alteration products extend is unknown. However, Parry (1976) has estimated that the first appearance of K-feldspar should occur at 200 meters and he observed that montmorillonite began to decrease at a depth of 60m. Hence, it is possible that the contribution of clay minerals to low values of resistivity may be minimal at a depth of order 500m. Crosby (pers. com.) confirms that clay alteration is not evident in the deeper sections of the wells drilled to date by Phillips Petroleum Company.

Montmorillonite has a high ion exchange capacity which leads to high mineral surface conductivity (Ward & Fraser, 1967). Pyrite also will increase the conductivity as will the presence of water below the water table. We would thus conclude that the surface materials would be reasonably resistive down to 105' (32m) whereafter the resistivity would drop rapidly. Schlumberger vertical electric sounding (Tripp and Ward, 1976) has roughly confirmed this type of geoelectric section at 100W, 3500N, approximately at the location of DDH1B of Figure 47. In Figure 48, we show the parameters, and their percent standard deviations for a layered earth model obtained by inversion of Schlumberger vertical electrical

sounding data. The first two layers of this model may be combined to yield 35m of resisitive material overlying a conductive layer. Further discussion of the limitations of the geological/geophysical correlation are contained in Tripp and Ward (1976) and in a later section of this report.

3.1.3 Hydrology

The pseudosections of Figures 1 through 41 and 49 through 51 and 53 demonstrate that while low resistivities occur near surface in the general area of the Dome and Negro Mag Faults (hereinafter referred to as the *convective hydrothermal system*, low resistivities also occur at depths of 100m to 300m to the west, especially beyond 800W. The lowest resistivity encountered anywhere was 1 Ωm and was measured with 1km dipoles near the railroad track on the line 4000 N (see Figure 40). Two explanations for such low resistivities are offered.

First, prehistoric Lake Bonneville sediments contact the alluvium at the 5100 foot elevation. The *interpreted* shoreline of ancient Lake Bonneville has been sketched in Figure 46. The presumed Bonneville shoreline seems to coincide with the 2 Ωm contour of the pseudosection of Figure 40. Our measurements on Lake Bonneville sediments near Abraham Hot Springs (Johnson, 1975) characteristically reveal resistivities less than 5 Ωm. Bonneville sediments could occur beneath the recent alluvium.

Second, brine may be assumed to have leaked, or is leaking, from the convective hydrothermal system. Evidence of past leakage is plentiful in the form of silica-cemented alluvium well west of the baseline in Negro Mag wash and in several other minor washes draining westward. A specific example occurs at 1500 W on line 8900W. A recent four-day flow test by Phillips Petroleum Company, of as much as 3 cu ft./sec., involved flow westward in Negro Mag wash; this brine all disappeared into the soil prior to reaching 2500W. Thus, we would reason that the surficial alluvium would be resistive, as observed, but that deeper alluvium would be brine-saturated and hence of low resistivity, also as observed.

Fault 5 of Figure 47 is based on photointerpretation of displacements in alluvium. As such it is weakly supported. However, the resistivity contours of Figures 44 and 45 would support the contention that this interpreted fault is a major conduit for brines leaking out of the convective hydrothermal system. There would appear to be no particular reason why the east-west fractures of Figure 47 should not leak brine westward also. In the past, both surface and subsurface westward leakage of brine seems to have occurred.

We know that the fresh water flow from the Mineral Range Mountains to the east of the area depicted in Figure 47 is substantial because fresh water springs are numerous at the base of the mountains. This water is probably carried, by the east-west fractures, westward to mix with the hot saline waters of the convective hydrothermal system. The east-west fractures of Figure 47 are not, for the most part, clearly defined by resistivity because most of our resistivity lines were oriented east-west. Faults 2 and 4, on the other hand, were defined mostly on the basis of resistivity data obtained on north-south lines. We are led to believe that additional east-west fractures may be delineated if additional resistivity surveying is conducted on north-south lines.

3.1.4 Interstitial and Fracture Porosity and Effects of Clay Alteration

The resistivity of near-surface geologic materials is largely determined by the electrical properties of the water contained in the pores, cracks, and larger joints and fractures. Important exceptions occur in the cases of clay minerals and the conducting oxides and sulfides. A useful empirical relation between the rock resistivity and the resistivity of the contained water is known as Archie's law

$$\rho_r = \rho_w \phi^{-m}$$

where ρ_r = resistivity of the rock

ρ_w = resistivity of the water

ϕ = fractional porosity

and m is an exponent usually near 2. The porosity of rocks and soils varies widely, from much less than 1% to greater than 50%. The resistivity of pore waters also varies considerably, typically from .1 Ωm to 10 Ωm. The resistivity of electrolytic solutions is approximately proportional to the concentration of dissolved ions, and resistivity decreases with temperature for moderate temperature increases. At much higher temperatures, near the critical point of water, the resistivity increases with temperature (Quist and Marshall, 1969).

Archie's law illustrates the very strong influence of porosity on resistivity. The porosity in rocks can be separated into various contributions depending on size and geometry. At the small end of the scale there are pores (rounded or tubular openings) and micro cracks (thin and often planar openings). At the large end of the scale there are macro cracks such as joints and fractures. For small scale features, the laboratory studies of Brace and his coworkers (Brace et al., 1965; Brace and Orange, 1968; Brace, 1971) have shown the effects that crack and pore porosity have on the resistivity of rocks. In general the crack porosity can be an important contribution at low pressures where the cracks are largely open. At pressures above a few kilobars most of the cracks close and the porosity is mostly pore porosity. The effects on the resistivity are as follows: as the cracks close in the low pressure region the resistivity may rapidly increase by an order of magnitude in a few kilobars, at higher pressures where most of the cracks are closed the rate of increase levels off to about 10% per kilobar. Effective pressures of the order of a few kilobars correspond to depths of about 5 to 10km, so

the rapid change in resistivity due to crack closure is expected to take place in this depth range. Since the resistivity increase with pressure due to crack closure is most likely greater than the decrease of solution resistivity due to temperature increase with depth, the net effect is expected to be an increase in resistivity with depth.

It was generally thought (Brace, 1971) that large scale jointing and fractures would have an important effect on the in situ resistivity, at least in the near surface, where such macro cracks would be largely open. However, recent work by Madden (1974) has shown that at many sites the joints and fractures do not contribute significantly to the conductivity. It was suggested in this latter work that this occurs because the joint porosity as an overall average is low. An added complexity is the effect of surface conduction, which is an important factor for very thin cracks and relatively dilute pore solutions. The process of surface conductivity makes thin cracks much more effective conduction paths than thick cracks. This is not to say that jointed and fractured rocks will not have a lower resistivity, because the very processes that give rise to jointing and fracturing (i.e., stress relief) on the macro scale also produce cracks on the micro scale. What it does seem to indicate is that the micro cracks dominate in determining the resistivity.

In geothermal areas the pore solutions tend to be more concentrated and this will tend to reduce the effects of surface conduction. It may be that in such areas, the larger cracks will contribute more to the overall lowering of the resistivity.

The closing of large scale joints and fractures with depth has been estimated by Brace (1971) based on the measured flow rates in granites and gneisses reported by Snow (1968), to occur at depths of the order of 100m. However, we should probably at this point discriminate between fractures and

and joints as thick cracks and fracture and fault zones which are known to be permeable flow zones to much greater depths.

In the deeper parts of geothermal areas we might also consider the effects of thermal stresses. The work of Madden (1974) indicates that thermal stressing creates micro cracks that are on the average much thicker than micro cracks due to mechanical stresses. Where surface conduction dominates, thermally created micro cracks will be relatively inefficient in lowering the resistivity. On the other hand, if pore solution concentrations are large, thermally induced micro cracks could contribute significantly to the lowering of the resistivity.

The presence of clays in rocks tends to reduce the resistivity because of the contribution that exchangeable cations can make to the current flow. For a fixed number of exchangeable cations the contribution to the total current will decrease as the concentration of the pore water increases. Therefore, the effects of clays are most pronounced in dilute solutions. Waxman and Smits (1968) extended the earlier work of Hill and Milburn (1956) and developed a simple model for the contribution of exchangeable clay cations to the electrical conductivity. Their expression for the resistivity of a clay bearing rock is

$$\rho_r = \frac{\rho_w F^*}{1 + \rho_w BQ}$$

where ρ_w is the resistivity of the bulk pore water, B is a factor which takes into account the dependence of the mobility of exchange cations on the pore water concentration, Q is the clay cation exchange capacity per unit pore volume and F* is the formation factor at very high concentrations where the effects of clays can be neglected. In this region F* can be expected to obey an Archie's law type of dependence on porosity.

Laboratory measurements on core samples from the clay alteration zone (30m to 60m) in hole 1A at Roosevelt Hot Springs KGRA show resistivities as low as 3-5 Ωm

(25°C, concentration and 5 x 10^3 ppm NaCl). These samples have porosities in the range from 15 to 35%.

Measurements over a range of concentrations of saturating solution can be used to deduce the cation exchange capacity (Q) for these samples. The range of Q for the highly altered samples is 0.5 to 1.0 meq/cm^3, which is in reasonable agreement with the clay determinations and chemical analyses. With this information we can estimate that the effect of the clays at porewater concentrations of 5 x 10^3 ppm is to reduce the resistivity by a factor of about 2 to 4. At higher clay contents or lower concentrations the effects would be larger.

The effects of temperature in this model have not been investigated. If the mobility of the clay exchange cations has the same temperature dependence as the free ions, then the factor $\rho_w B$ will be relatively insensitive to temperature for concentrations of the order of 10^3 ppm. The temperature effect will then be to first order, the same as for Archie's law.

3.1.5 Heat Source

The youngest rocks known to exist in the immediate vicinity of Roosevelt Hot Springs are the silicic volcanics exhibiting ages between 500,000 and 700,000 years (Lipman et al., 1975). Evans and Nash (1975) demonstrate that the lavas were erupted at temperatures in the range 670-760°C. If we assume that an intrusive equivalent of these rocks occur beneath the Mineral Range, then it's maximum paleotemperature would also lie in this range. These rocks would begin to solidify at a temperature no less than 650°C and would be cooled where in contact with water to a temperature of no more than 283°C according to the Na-K-Ca geothermometer (Parry, 1976) and possibly as low as 269°C which is the hottest temperature encountered in drilling. (Crosby, pers. com.)

Hot *dry* silicic rocks with no molten phase, at temperatures below 650°C, exhibit resistivities in excess of 10^6 ohm meters (Keller and Frischknecht,

1966, p. 10). From the above discussion, we conclude that hot *dry* rock, with no molten phase, would not exhibit a marked resistivity low.

On the other hand, if a silicic rock is molten and contains water vapor at sufficient pressure, it may exhibit a resistivity as low as 1 Ωm (Lebedev and Khitarov, 1964). The question then arises, "Is molten silicic rock still present at depths within the range of the 1 km dipole-dipole resistivity surveys used?" The depth of exploration obtained with 1 km dipole-dipole profiles, with values of n to 6, may be estimated as 1.5 km using the work of Roy and Apparao (1971) as a guide.

If hot molten rock occurs at depth, it might be surrounded by a resistive steam phase and then by a conductive hot water phase.

The qualitative discussion of the detectability of heat sources shall be tested quantitatively in the next section. Crosby (pers. com.) has stated that, in his opinion, the heat source has been detected by MT as a resistivity decrease, at a depth of 5 to 6 km to values less than 1 Ωm.

3.2 Quantitative

3.2.1 Two-Dimensional Resistivity Modeling

A two-dimensional transmission-surface forward algorithm was utilized to calculate theoretical dipole-dipole resistivity pseudosections to which the observed pseudosections could be compared. Figures 49 through 54 illustrate both the comparisons of observed and theoretically generated pseudosections and the theoretical models used in the calculations. In generating both the observed and theoretical pseudosections we combined 100m and 300m dipole data for Figures 49, 50, and 53 while we combined 300m and 1km dipole data for Figure 51. It is useful to combine data sets from different dipole lengths since some parameters of the two-dimensional models are better determined in one data set than in another.

The theoretical, or model, pseudosection of Figure 49 is a reasonable match to the observed pseudosection. The 5 Ωm low resistivity zone centered at 400 W on Line 1000N defines the fracture zone bounded by the Dome Fault on the west and Fault 1 on the east. This 5 Ωm zone is surrounded by a 650m wide 10 Ωm zone. Resistivities in excess of 50 Ωm occur at a depth of about 450m. A 300m by 300m cross-section of 5 Ωm occurs beneath 300 E and probably represents faults at depth there. Resistivities as low as 10 Ωm occur at a depth of 100m westward of 1000 W.

In Figure 50, pertaining to Line 3000N, the surficial 5 Ωm zone is centered over the Dome Fault and the 10 Ωm zone surrounding it extends mostly eastward. A 5 Ωm zone also is centered beneath 600 E at a depth of 100m and it is contiguous with a 10 Ωm zone which extends beyond 1200 E and extends to at least 500m. Several faults mapped in Figure 47 seem to be contributing to these latter features. As before, 10 Ωm material exists beneath 200 m depth west of 600 W.

Figure 51, portraying deeper exploration than did Figures 49 and 50, reveals that the whole geolectric section bottoms in 300 Ωm material. The surficial 5 Ωm zone, surrounded as usual by a 10 Ωm zone, coincides with the fracture zone between Dome Fault and Fault 1. To the west, at a depth of 300m, 5 Ωm and 10 Ωm material occurs. The data, taken on Line 4000N, gives no hint of highly fractured or molten rock below 600m beneath or to the east of the convective hydrothermal system.

Figure 52 shows the observed and calculated pseudosections for the model in the bottom of the figure. The results show an increase in resistivity with depth and toward the east as the line traverses the granite of the Mineral Range. A very interesting feature is the vertical conducting block between 6E and 7E. This is the region of the saddle on Negro Mag Wash and a line drawn between the volcanic features Bearskin Mountain and Crater Knoll passes between these stations. This could be an indication of a fracture system running between these two features. Additional modeling indicates that the conductive zone probably extends to at least 600m and it could be considerably deeper.

Figure 53 portrays data and a model for Line 8100N. From the base line to 500E a 10 Ωm zone occurs at surface or at very shallow depth. This zone correlates with Fault 3 but it is bottomed at 200m by 100 Ωm material. From 500 E to 1000 E, 20 Ωm material exists to 200m depth; this zone is probably related to another fracture depicted in Figure 47. To the west, low resistivity material occurs from surface to a depth of at least 500 m.

The above two-dimensional models are interpreted as follows:

1) The north-south fractures are conductive to depths of order 500m.
2) The low resistivities of the fractures are attributed either to clay and pyrite alteration or to hot brine in the fractures or to both.
3) The marked increase in resistivity at about 500m is attributed

either to a reduction in alteration, to the replacement of brine by steam, or to tightening of the fractures, or to lack of resolution of low resistivity features below 500m.

4) Tightening of the fractures at about 500 m is possible but we have no definitive information on such.

5) While a reduction in alteration with depth seems like the most probably cause of the increase in resistivity with depth, the induced polarization method is required to prove this point. Once induced polarization data is obtained, the percent frequency effect may be modeled in two dimensions by the 2D transmission surface forward algorithm. If the resistivity and percent frequency effect models do not agree, then any resistivity low not accompanied by an induced polarization anomaly may be attributed solely to brine-filled fractures.

6) Subsequently we shall establish that low resistivity zones occurring below 500 m might be beyond limits of resolution of current interpretation techniques.

7) The convective hydrothermal system is leaking brine westward to produce low resistivities at depths of 100m to 300m.

3.2.2 Resolution of Two-Dimensional Resistivity Modeling

The five theoretical geoelectric sections used above to obtain model pseudosections with which to compare observed pseudosections, were obtained by guessing models, iteratively, which might afford matches between observed and theoretical pseudosections. Each model used has a large number of parameters. Had we the algorithms available, we would have utilized inversion to establish the resolution of the parameters (e.g., Inman, 1975). Lacking such inverse algorithms, we tested resolution by inserting more model elements in our forward algorithm. This section intends to portray the testing of reso-

lution via simple-minded forward algorithms.

3.2.2.1 Variations on the Basic Model

Figure 54 shows the basic model for the 4000N line, from 5 km West to 5 km East and variations thereon. To the east of the baseline (0), the near surface part of the geothermal system is modeled by a 5 to 10 Ω-m zone extending to a depth of 600m. The effects of more deeply buried features is modeled by assigning resistivity values to the lettered blocks. Blocks A,B,C,D are outlined in solid lines and blocks E,F and G in dashed lines.

In the basic model (Figure 54A) pseudosection, all the blocks have a resistivity of 300 Ω-m, the same as the rest of the background, corresponding to Figure 51. The first variation that was tested was a very resistive (steam?) region, just below the conductive region. For this test, block A was set to 10^4 Ω-m and the pseudosection (not shown) is essentially the same (variations less than 10%) as the basic model. So we can conclude that a much more resistive bottom zone (greater than 300 Ωm) is not detectable by these measurements.

Next, a good conductor at depth was modeled by setting B and C equal to 1 Ω-m and 10 Ω-m, respectively, and the pseudosections for these two cases are shown in Figure 54 C and D. In the first case (B=C=1 Ω-m) we see that the apparent resistivities in the resistivity high just below 1E and 2E are reduced by a factor of about 2. Certainly this is a noticeable change in the pseudosection. For a lesser contrast (B=C=10 Ω-m) the effects on the resistivity high are reduced, about a 25 percent reduction in the maximum values. The results for this latter model are also essentially the same as that for a more conductive block buried deeper, i.e., the case of C=D=1 Ω-m.

In either of these latter models, B=C=10 Ωm or C=D=1 Ωm, the reduction of the apparent resistivity values is significant, but they might be considered near the limit of detectability considering other perturbing effects such as non-2-dimensionality.

Another test case was run with B=C=1 Ω-m, but surounded by a resistive layer (10^4 Ω-m) 250 m to 400 m thick (a good conductor surrounded by a steam zone). In this case the resistive zone "shielded" the conductive zone and the pseudosection was essentially the same as the basic model.

The last series of test cases involved the blocks E,F and G in order to see what effects a conductive zone extending to great depth (2.0 km) would have. In the first case, for E = 10Ωm, (a thin fracture zone extending to depth) the apparent resistivities near the high were lowered by a small amount generally less than 10%. With E=F=10 Ω-m the changes were slightly larger and with E=F=G=10 Ω-m the maximum changes rose to about 25%, but were still not as drastic as that shown in Figure 54D.

In conclusion we can say that a more resistive zone at depth or a thin (~250m) conductive zone extending below the near surface zone probably would not be detectable by the 1 km profiling. Also a conductive zone of the order of kilometers in size buried at depths below 1 km and surrounded by a resistive zone would probably not be detectable. On the other hand a large (several/ kilometers on a side) conductive zone (1 to 10 Ωm) buried at depths of 1 to 2 km should be detectable. Since the effects of such conductive blocks are not observed we might conclude that they are not present at depth. This conclusion should be tempered with the knowledge that in 2-dimensional modeling the large number of degrees of freedom in the parameters of the model might permit one to "model out" a deep seated source with near-surface perturbations.

3.2.3 One-Dimensional Resistivity, Temperature, Salinity and Porosity Modeling.

Figure 55 shows the electrical model derived by inversion of Schlumberger sounding on the 3500N line (100W). Also, shown is a temperature profile estimated from nearby thermal gradient measurements, and three resistivity curves derived from Archie's law. The resistivity curves are derived assuming a salinity of 5×10^3 ppm, (NaCl) the estimated temperatures, and three porosities 25%, 10% and 5%. In looking at the model derived from the Schlumberger sounding data we see a sharp drop in the resistivity associated with the water table at around 35m, a low resistivity zone to about 400 m and then an increase in resistivity to greater than 100 Ωm. The curved derived from Archie's law using a porosity of 25% gives the right order for the observed resistivity in the conductive zone. Since this curve does not take into account the effect of clays which are probably present, the porosity is probably somewhat less than this value. Including the effects of clays will result in similar curves but with reduced porosities, since to first order the effects of temperature are the same whether or not clays are present. The abrupt increase in resistivity at a depth of 400m might have several explanations as noted earlier. One, the reduction in pore water due to the presence of steam displacing the liquid phase, does not seem likely in view of the estimated temperature and pressure. Assuming a hydrostatic head, the presssure is in the range of 30-40 atmospheres. At this pressure, the water-steam phase transition takes place at the temperature of 240°-250°C. This would imply a linear temperature gradient in excess of 600°/km since the resistivity appears to rise abruptly at about 400-500m. While such temperature gradients have been observed here in holes less than 100m, they would not be expected to continue to 400-500m. Other possibilities include the reduction in clay (or sulfide) content, change in water salinity, and a change in porosity. A change in resistivity by a factor

often does not seem too likely to be caused by a change in clay content since the pore fluid is already quite conductive. Since the resistivity is such a strong function of porosity perhaps this might at first be considered the most likely candidate. The porosity might change by closure or absence of cracks and fractures, cementation or by a lithologic change. A simple explanation might be the change from alluvium to bedrock and the change from 25% porosity to 5% porosity is about what would be expected. This explanation would, then require about 300-500 m of alluvial fill to the east of the upthrown block on the dome fault.

The wells 54-3 and 13-10 drilled by Phillips Petroleum Company encountered bedrock at 285 feet (87 m) and 210 feet (64 m), respectively. The latter hole encountered highly altered rock to 270 feet (82 m). Clearly, the drilling does not support the above interpretation.

As noted earlier, the measured effects of the clay on core samples from the altered zone are to reduce the resistivites by factors of 2 to 4. The removal of the clay, *without changing the porosity,* would then lead to an increase in the resistivity by this amount. This by itself would not account for the change seen at depth, which is at least a factor of ten. However, the alteration to clays could well be accompanied by an increase in porosity and these two effects of the alteration might easily explain the large change in resistivity.

The geochemical studies of Parry (pers. com.) indicate that as depth and temperature increase the hydrothermal system should pass from the clay alteration regime into a K-Feldspar stable regime. Estimates of the depth for this transition are in the range from 200 to 400m, in reasonable agreement with the bottom of the conductive zone as determined by the resistivity sounding. This transition would account for the lack of clays at depth, thus increasing the resistivity, and the secondary deposition of K-Feldspar at depth might further reduce the porosity leading to additional increases in the resistivity.

It would seem, therefore, that the decrease in clay content and/or the lack of resolution of the resistivity method are the most likely culprits responsible for our inability to map, electrically, the convective hydrothermal system at depths below about 500m with the electrical methods.

4.0 Comparison of bipole-dipole and dipole-dipole resistivity techniques.

The area covered by dipole-dipole resistivity was earlier covered, for Phillips Petroleum Company, by a bipole-dipole resistivity survey. Four 3 km bipole source locations were used. Vector electric fields were measured at 1.5 to 2.0 km intervals on roughly a square grid.

This survey drew attention to the low resistivities in Milford Valley but did not locate any recognizable resistivity lows over the convective hydrothermal system. The 1 km dipole-dipole survey located only a very small resistivity low over this system. Hence one can conclude that large source and receiver lengths and large source-receiver separations are not adequate to resolve the convective hydrothermal system. Further, these large spread systems both failed to detect the resistive alluvial overburden.

The 100 m and 300 m dipole-dipole surveys both clearly detected the top 500 m of the convective hydrothermal system, but failed to detect the deeper parts of the system,if such are of lower resistivity, according to our modeling studies. The design of resistivity surveys for the geothermal environment evidently requires considerable care. Detailed dipole-dipole resistivity surveys can be very effective, in a supporting role for three-dimensional geologic mapping. It is not obvious that the bipole-dipole technique is of value at Roosevelt Hot Springs KGRA.

5.0 Conclusions

While the resistivity method has been quite useful in mapping fractures to depths of order 500 m in the vicinity of the convective hydrothermal system at Roosevelt Hot Springs KGRA, and while it has given useful geoelectric sections to depths of order 1 to 2 km, it has evidently failed to map the convective hydrothermal system at depths greater than about 500 m. The shorter dipole spreads of 100 m and 300 m are more useful than 1 km spreads in this environment.

In considering the depth extent of conductive bodies, many model studies have shown that once the conductive block has a depth extent several times its width, further increase in the depth extent produces little additional change in the pseudosection. This is a typical example of "saturation," due to the fact that most of the effects are due to the upper portions of the conductive block.

In the base model of section 3.2.2 the width and depth extent are approximately the same, so there is the possibility of detecting measureable changes due to an increase in depth extent. In fact, increasing the depth extent to 2 km of a zone as broad as the near-surface conductive zone produces an effect which should have been detected. Since these effects are not seen in the observed pseudosection we can probably conclude that the depth extent of the broad conductive zone is not much greater than 500 m. On the other hand the model studies also show that if the deeper portion is much thinner than the near surface zone it not be resolved by the 1 km profiling.

Large conductive (1 to 10 Ωm) zones of the order of kilometers on a side buried at depth between 1 to 2 km would probably be detectable by the 1 km dipole profiling. If such a conductive zone is considered as a model of a not rock source (molten, partially molten or solid), then there is no evidence for such a source. On the other hand, one might reasonably expect such a source to occur at greater depths beyond the range of investigation in the

studies completed so far. Also such a hot rock source might be surrounded by a resistive region (vapor dominated or above the critical point) in which case the conductive target might be effectively "shielded."

Deeper probing by using larger dipoles was investigated by computing the pseudosection for the basic model using 3 km dipoles. The major effect noted in the pseudosections is that due to the contrast in resistivity between the valley fill and the mountains. A conductive block (1 Ωm), extending from the baseline to 3 km east and a depth extent of 2.4 km to 5 km was then inserted in the basic model, in order to model a large conductive zone at depth. The major effect was to reduce the apparent resistivities at depth by about 50% in a zone extending from just west of the baseline to about 6 km east. In this test such a conductive block would probably be detectable.

The convective hydrothermal system must have leaked, or is leaking, westward since exceptionally low resistivities are encountered well above the apparent shoreline of prehistoric Lake Bonneville, east-west and northwest-southeast fractures appear to carry brine westward into the center of Milford valley. East-west fractures quite possibly bring cold and hot waters into the convective hydrothermal system. There is, therefore, a need to delineate these east-west fractures.

It is entirely possible that the source of heat lies north, south or east of the convective hydrothermal system. Based on our knowledge of thermal gradients (Sill and Ward, 1976), it is unlikely to lie to the west.

More field work, recommended in section 6.0, it necessary before the utility of the dipole-dipole resistivity method may be evaluated fully in this class of geothermal occurrence.

The bipole-dipole method, when used in its characteristic reconnaissance manner, has not helped define the convective hydrothermal system at Roosevelt Hot Springs KGRA.

6.0 Recommendations

The following resistivity/induced polarization surveys are warranted on the basis of discussions presented above.

1) Resistivity surveys using 100 m and 300 m dipoles should be conducted on north-south lines to the east and west of the Dome Fault to attempt to delineate east-west fractures important to recharge and discharge of the convective hydrothermal system. These surveys should be designed using Figure 47 as a model.

2) Four resistivity profiles located 2 km and 4 km north and south of the established grid should be completed using 300 m dipoles in an attempt to determine the north-south extent of the convective hydrothermal system.

3) A 300m dipole resistivity traverse should be conducted from 0 km E to 10 km E on Line 4000N to delineate the interpreted conductive zone at 6.5 km E as shown in Figure 52. Wherever topography permits it, additional traverses should be established.

4) Induced polarization traverses should be conducted using 100m and 300m dipoles on Lines 1000N, 3000N, 4000N, 5950N, and 8100N from approximately 1500 W to 1500 E to determine the contribution that clay and pyrite alteration makes to the pattern of low resistivities in the vicinity of the convective hydrothermal system.

5) A resistivity profile utilizing 3 km dipoles should be obtained on Line 4000N from 9 km W to 12 km E.

7.0 Acknowledgements

This research was funded under NSF Grant GI-43741. We are indebted to Ritchie Corryell for his initial faith in our abilities, for his testing of us by external review panels, and for his continued counsel, interest, and advice.

Dr. C. M. Swift, Jr., provided the 2D transmission surface algorithm we have used abundantly in this report. Terry Crebs and Mark Halliday, graduate students in this department, supervised the collection of most of the field data.

Richard C. Lenzer and Gary W. Crosby of Phillips Petroleum Company have been most helpful in providing depth of bedrock in selected wells and in allowing us use of their bipole-dipole resistivity data. We are grateful to them and to Phillips Petroleum Company.

REFERENCES

Brace, W. F., A.S. Orange, and T. R. Madden, 1965, The Effect of Pressure on the Electrical Resistivity of Water-Saturated Crystalline Rocks, J.G.R., Vol. 70, No. 2, p. 5669-5678.

Brace, W. F., and A. S. Orange, 1968, Further Studies of the Effect of Pressure on Electrical Resistivity of Rocks, J.G.R., Vol. 73, No. 16, p. 5407-5420.

Brace, W. F., 1971, Resistivity of Saturated Crustal Rocks to 40 km Based on Laboratory Measurements, in The Structure and Physical Properties of the Earth's Crust, AGU Geophysical Monograph 14, p. 243-256.

Evans, S. H. Jr., and W. P. Nash, 1975, Mid and Late Cenozoic Volcanism in Southwestern USA, Abstracts, GSA Annual Meeting, Salt Lake City, Oct. 20-22.

Hill, H. J., and J. D. Milburn, Effect of Clay and Water Salinity on Electrochemical Behavior of Reservoir Rocks, Petroleum Trans. AIME, 207, 65, 1956.

Inman, J. R., 1975, Resistivity Inversion with Ridge Regression, Geophysics, Vol. 40, No. 5, p. 798-817.

Johnson, E. H., 1975, Resistivity and Induced Polarization Survey of a Basalt Flow in a Geothermal Environment, Western Utah, M.S. Thesis, Department of Geology and Geophysics, University of Utah.

Keller, G.V., and F. C. Frischknecht, 1966, Electrical Methods in Geophysical Prospecting, New York, Pergamon Press.

Lebedev, E. B., and N.I. Khitarov, 1964, Dependence of the Beginning of Melting of Granite and the Electrical Conductivity of its Melt on High Water Vapor Pressure, Geochemistry International, v. 1, p. 193-197.

Lipman, P. W., Rowley, P. D., and Pallister, J.S., 1975, Pleistocene Rhyolite of the Mineral Range, Utah - Geothermal and Archeological Significance, Abstracts, GSA Annual Meeting, Salt Lake City, Oct. 20-22.

Madden, T. R., 1974, Near Surface Electrical Properties of Rocks as a Guide to Mechanical Properties, Final Report AFCRL-TR-75-0179, Dec. 31.

Nash, W. P., 1976, Mineralogy and Petrology of the Mineral Range Volcanics, Final Report NSF Grant GI-43741, In Preparation.

Parry, W. T., 1976, Alteration Studies, Roosevelt Hot Springs KGRA, Final Report, NSF Grant GI-43741, In Preparation.

Peterson, C. A., and J. A. Whelan, 1974, Geologic Map of the Roosevelt Hot Springs Area, Beaver County, Utah, Preliminary Report, Utah Geological and Mineral Survey.

Quist, A. S., and W. L. Marshall, 1969, The Electrical Conductances of Some Alkali Metal Halides in Aqueous Solutions from 0 to 800° and at Pressure to 4000 Bars, J. Phys. Chem., 73, 978.

Roy, A., and A. Apparao, 1971, Depth of Investigation in Direct Current Methods, Geophysics, Vol. 36, p. 943-959.

Sill, W. R., and S. H. Ward, 1976, Thermal Gradients in the Vicinity of Roosevelt Hot Springs, KGRA., Final Report, NSF Grant GI-43741, In Preparation.

Snow, D. T., 1968, Rock Fracture Spacings, Openings, and Porosities, J. Soil Mech. Foundations Div., Proc. Amer. Soc. Civil Eng., 94 (SMI), Pap. 5736, 73-91

Tripp, A. C., and S. H. Ward, 1976, Electromagnetic and Schlumberger Sounding, Roosevelt Hot Springs KGRA, Final Report, NSF Grant GI-43741, In Preparation.

Ward, S. H., 1976, Interpretation of Aeromagnetic Data, Roosevelt Hot Springs KGRA and Cove Fort-Sulphurdale KGRA, Final Report, NSF Grant GI-43741, In Preparation.

Ward, S. H., and D. C. Fraser, 1967, Conduction of Electricity in Rocks, Mining Geophysics, Vol. II, Tulsa, Society of Exploration Geophysicists.

Waxman, M.H., and L.J.M. Smits , Electrical Conductivities in Oil-Bearing Shaly Sands, Trans. Soc. Pet. Eng., 243 107, 1968.

List of Illustrations

Fig. 1. Pseudosection, Line 0015N, a=100m, 1:5000.

Fig. 2. Pseudosection, Line 0500N, a=100m, 1:5000.

Fig. 3. Pseudosection, Line 1000N, a=100m, 1:5000.

Fig. 4. Pseudosection, Line 1150N, a=100m, 1:5000.

Fig. 5. Pseudosection, Line 1500N, a=100m, 1:5000.

Fig. 6. Pseudosection, Line 2200N, a=100m, 1:5000.

Fig. 7. Pseudosection, Line 3000N, a=100m, 1:5000.

Fig. 8. Pseudosection, Line 3500N, a=100m, 1:5000.

Fig. 9. Pseudosection, Line 3800N, a=100m, 1:5000.

Fig. 10. Pseudosection, Line 4000N, a=100m, 1:5000.

Fig. 11. Pseudosection, Line 4300N, a=100m, 1:5000.

Fig. 12. Pseudosection, Line 4700N, a=100m, 1:5000.

Fig. 13. Pseudosection, Line 5000N, a=100m, 1:5000.

Fig. 14. Pseudosection, Line 5116N, a=100m, 1:5000.

Fig. 15. Pseudosection, Line 5400N, a=100m, 1:5000.

Fig. 16. Pseudosection, Line 5700N, a=100m, 1:5000.

Fig. 17. Pseudosection, Line 5950N, a=100m, 1:5000.

Fig. 18. Pseudosection, Line 6400N, a=100m, 1:5000.

Fig. 19. Pseudosection, Line 6500N, a=100m, 1:5000.

Fig. 20. Pseudosection, Line 7000N, a=100m, 1:5000.

Fig. 21. Pseudosection, Line 8100N, a=100m, 1:5000.

Fig. 22. Pseudosection, Line 8900N, a=100m, 1:5000.

Fig. 23. Pseudosection, Line 10000N, a=100m, 1:5000.

Fig. 24. Pseudosection, Line 11000N, a=100m, 1:5000.

Fig. 25. Pseudosection, Line 12000N, a=100m, 1:5000.

Fig. 26. Pseudosection, Line 0200E, a=100m, 1:5000.

Fig. 27. Pseudosection, Line BASELINE, a=100m, 1:5000.

Fig. 28. Pseudosection, Line 0200W, a=100m, 1:5000.

Fig. 29. Pseudosection, Line 0400W, a=100m, 1:5000.

Fig. 30. Pseudosection, Line 0700W, a=100m, 1:5000.

Fig. 31. Pseudosection, Line 1500W, a=100m, 1:5000.

Fig. 32. Pseudosection, Line 1000N, a=300m, 1:15000.

Fig. 33. Pseudosection, Line 2200N, a=300m, 1:15000.

Fig. 34. Pseudosection, Line 3000N, a=300m, 1:15000.

Fig. 35. Pseudosection, Line 4000N, a=300m, 1:15000.

Fig. 36. Pseudosection, Line 5950N, a=300m, 1:15000.

Fig. 37. Pseudosection, Line 8100N, a=300m, 1:15000.

Fig. 38. Pseudosection, Line 10000N, a=300m, 1:15000.

Fig. 39. Pseudosection, Line PASS ROAD, a=1km, 1:50000.

Fig. 40. Pseudosection, Line 4000N, a=1km, 1:50,000.

Fig. 41. Pseudosection, Line 5950N, a=1km, 1:50,000.

Fig. 42. Data plotting scheme Dipole-dipole array.

Fig. 43. Location of traverse lines, 100m dipoles.

Fig. 44. Contour map of 100m first separation apparent resistivity.

Fig. 45 Contour map of 300m first separation apparent resisitivity showing location of traverse lines.

Fig. 46. Location of traverse lines, Pass Road, 4000N, and 5950N used for 1km dipole survey.

Fig. 47. Fractures interpreted from resistivity, geology, photogeology, and aeromagnetics.

Fig. 48. Inverse interpretation of Schlumberger vertical electric sounding at 100W x 3500N.

Fig. 49. Observed and theoretical pseudosections plus theoretical model, Line 1000N.

Fig. 50. Observed and theoretical pseudosections plus theoretical model, Line 3000N.

Fig. 51. Observed and theoretical pseudosections plus theoretical model, Line 4000N from 4500W to 4500E.

Fig. 52. Observed and theoretical pseudosections plus theoretical model, Line 4000N from 1 km W to 10 km E.

Fig. 53. Observed and theoretical pseudosections plus theoretical model, Line 8100N.

Fig. 54. Resistivity resolution tests, Line 4000N from 5 km W to 5 km E.

Fig. 55. Schlumberger VES Model of resistivity ρ versus depth, (hachured step model), predicted ρ versus depth for porosities of 5%, 10%, and 25% including the effect of temperature increasing with depth.

Figures 1 through 38 will be made available upon special request but are deleted from the body of this report in order to reduce bulk and cost.

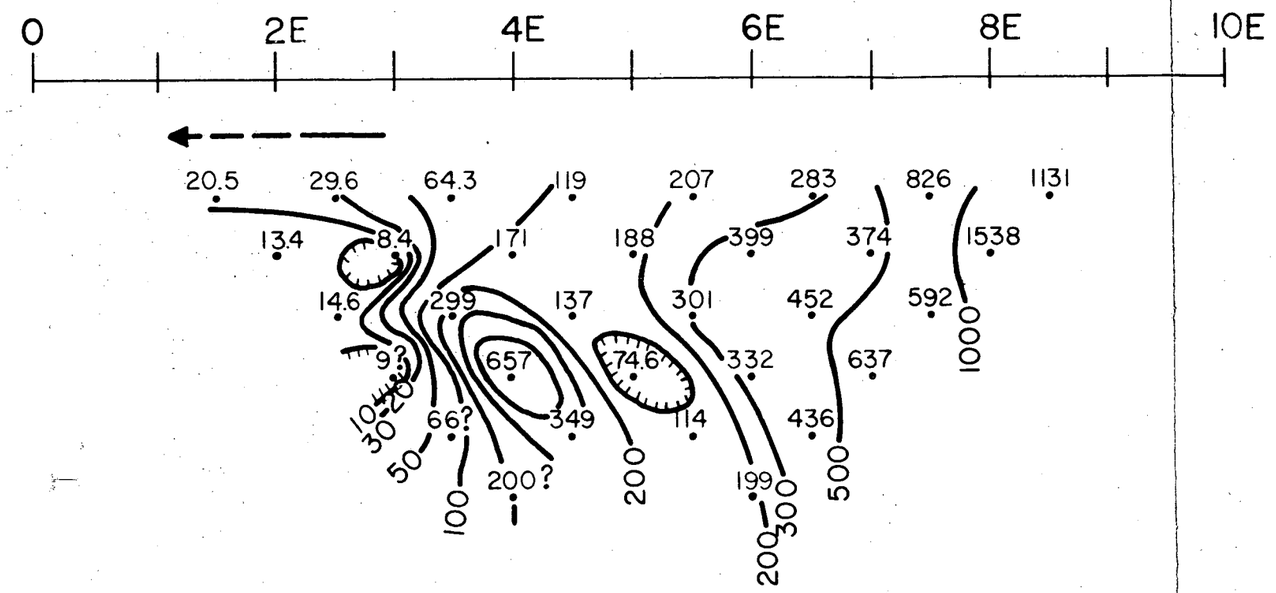

LEGEND

——— < 10Ω m

- - - - - 10-20Ω m

PASS ROAD Figure 39

PROJECT– KGRA
LOCATION – ROOSEVELT HOT SPRINGS
DIPOLE-DIPOLE RESISTIVITY— PSEUDOSECTION
SCALE – 1:50,000
a= 1 km CONTOURS AT 1,2,3,5,10....

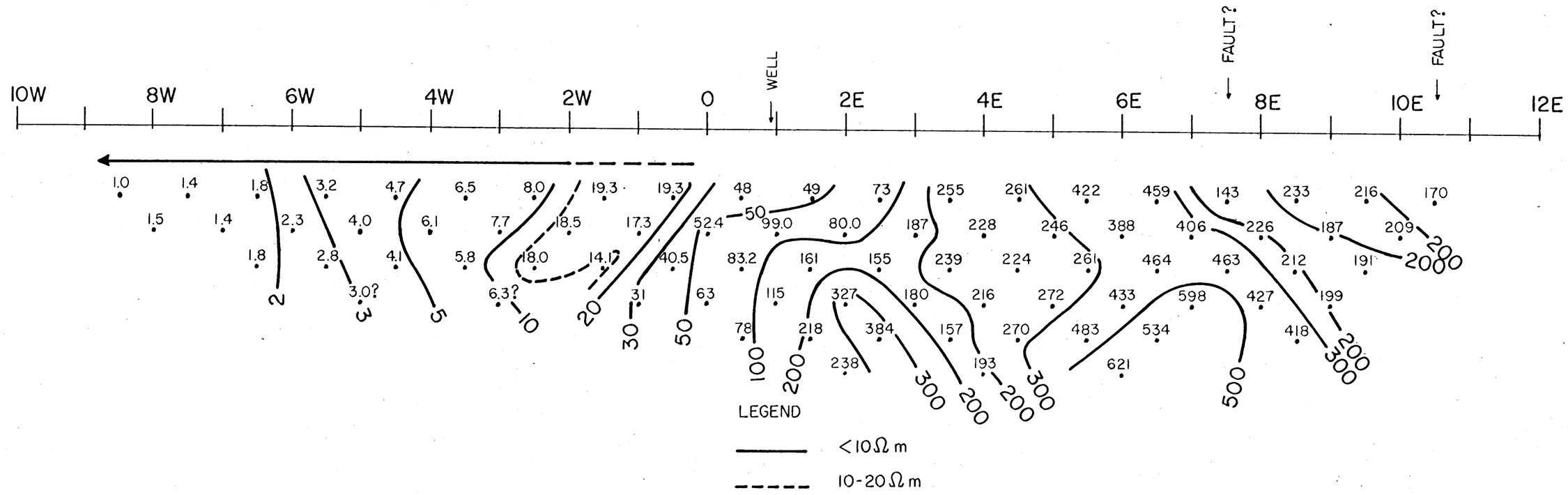

LINE 4000 N. Figure 40
PROJECT – KGRA
LOCATION – ROOSEVELT HOT SPRINGS
DIPOLE-DIPOLE RESISTIVITY — PSEUDOSECTION
SCALE – 1:50,000
a = 1 km CONTOURS AT 1,2,3,5,10....

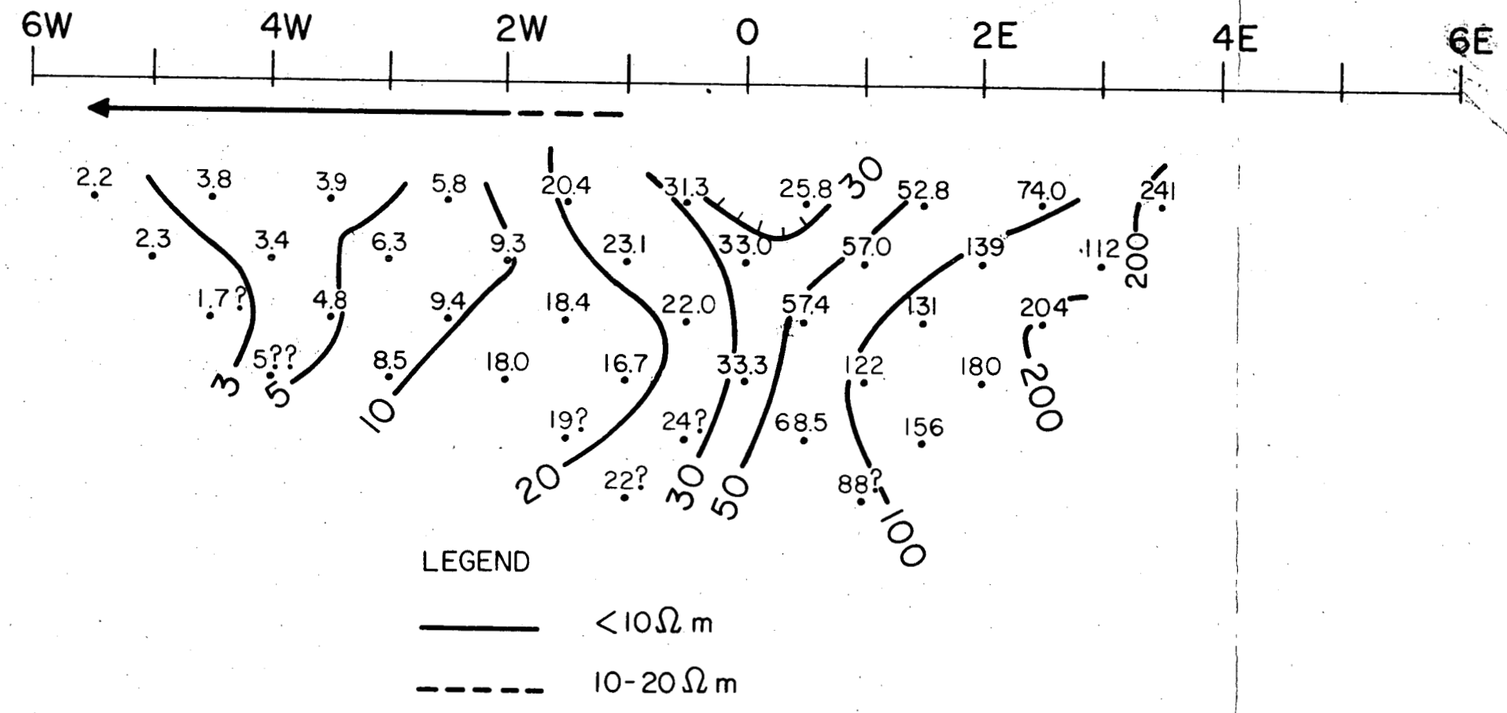

LINE 5950 N. Figure 41
PROJECT—KGRA
LOCATION—ROOSEVELT HOT SPRINGS
DIPOLE-DIPOLE RESISTIVITY— PSEUDOSECTION
SCALE—1:50,000
a=1km CONTOURS AT 1,2,3,5,10....

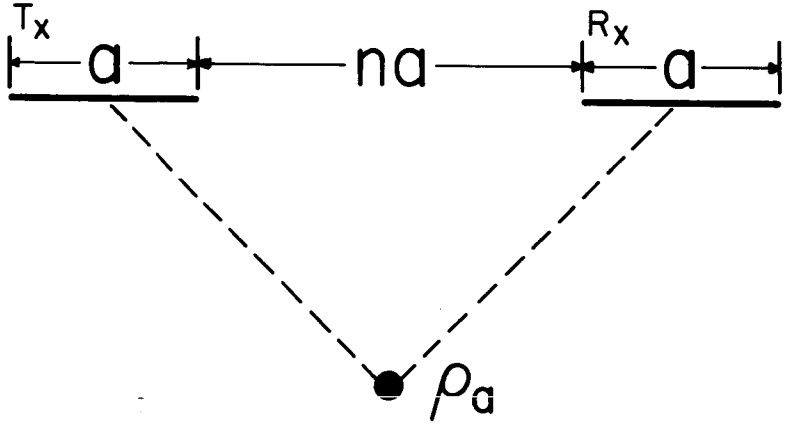

DATA PLOTTING SCHEME
DIPOLE-DIPOLE ARRAY

Figure 42

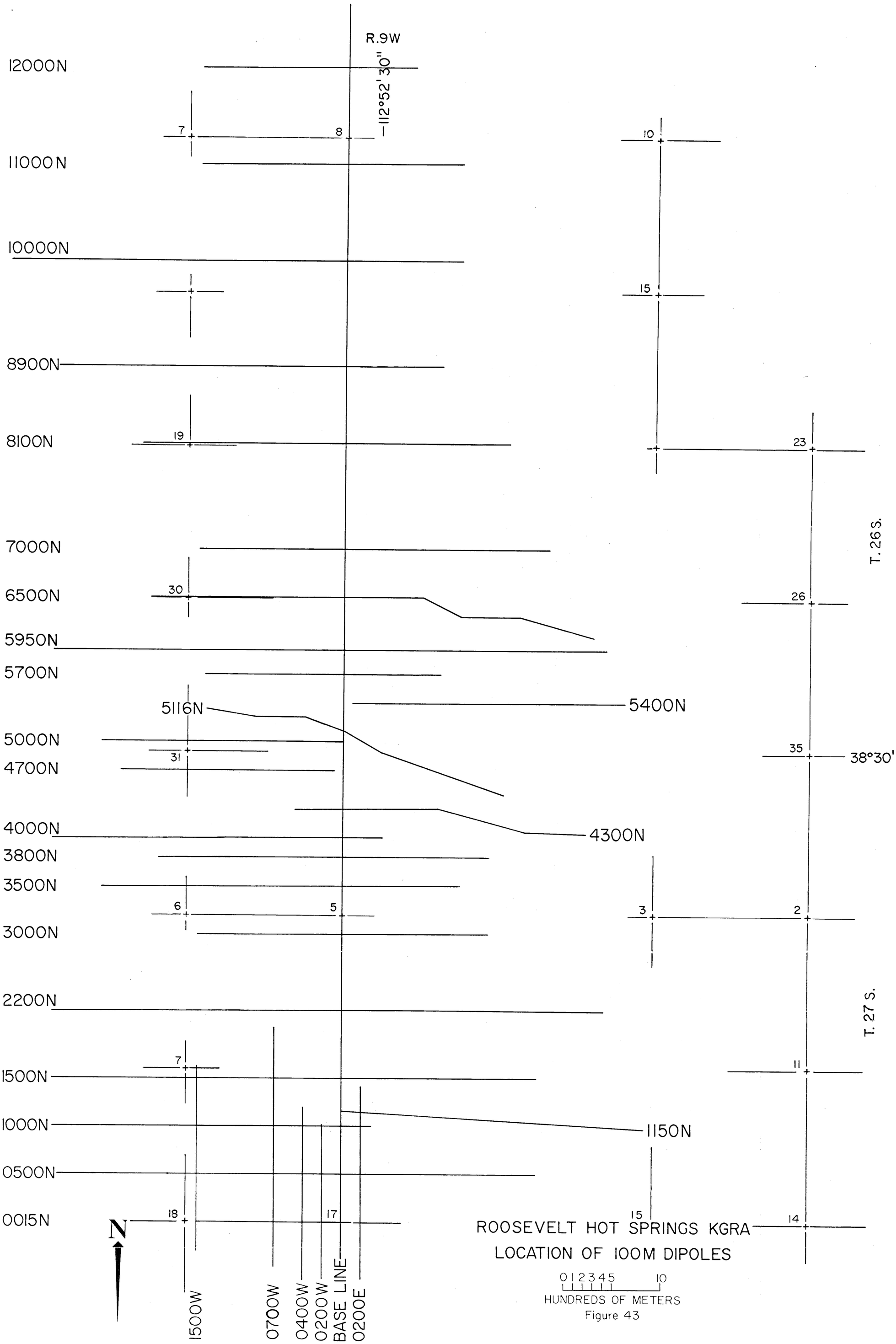
R.9W
112°52' 30"
12000N
11000N
10000N
8900N
8100N
7000N
6500N
5950N
5700N
5116N
5400N
5000N
4700N
4300N
4000N
3800N
3500N
3000N
2200N
1500N
1000N
0500N
0015N
7
8
10
15
19
23
30
26
31
35
38°30'
6
5
3
2
11
18
17
15
14
T. 26 S.
T. 27 S.
N
1500W
0700W
0400W
0200W
BASE LINE
0200E
1150N
ROOSEVELT HOT SPRINGS KGRA
LOCATION OF 100M DIPOLES
0 1 2 3 4 5 10
HUNDREDS OF METERS

Figure 43

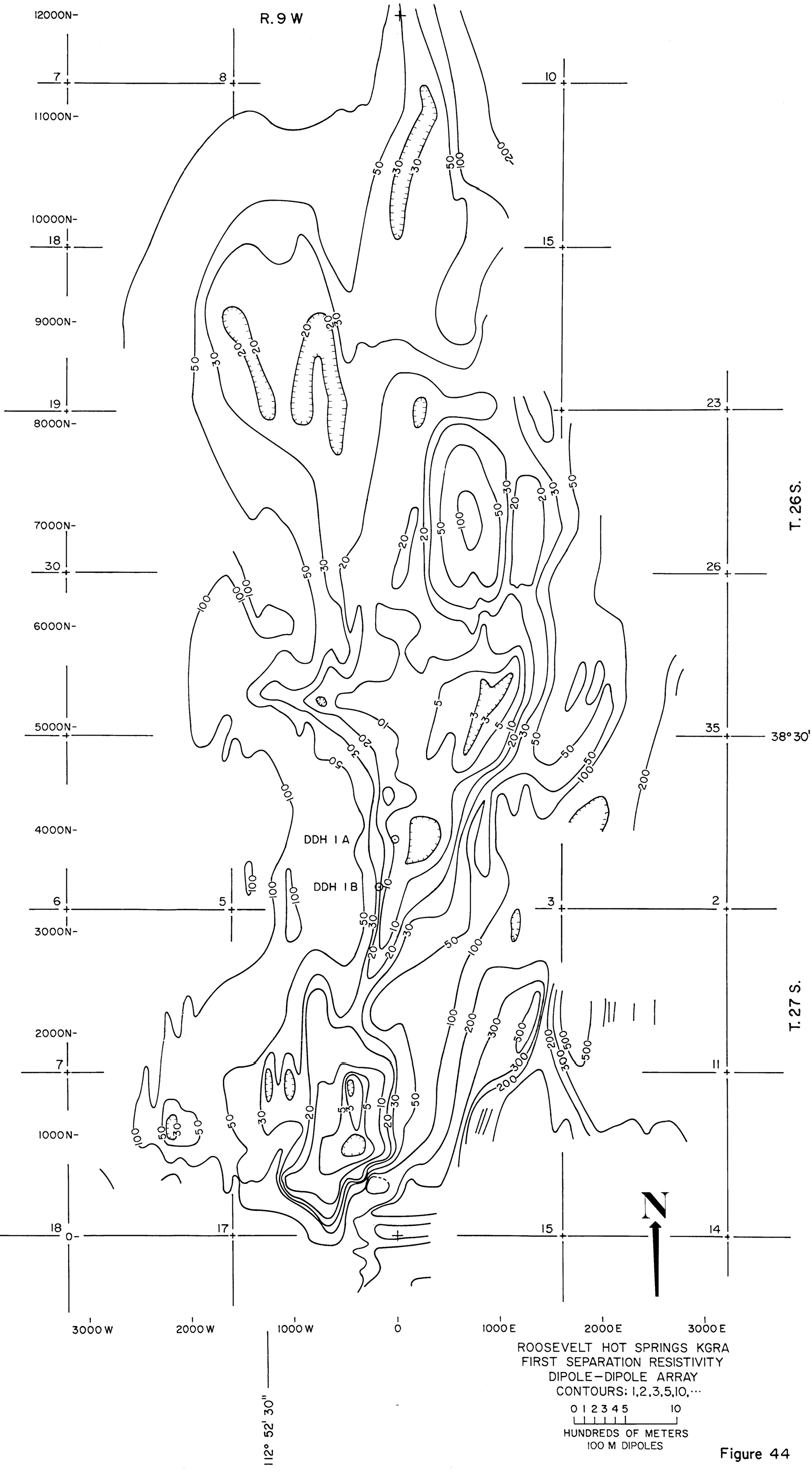
R.9 W
T.26S.
T.27 S.
38° 30'
112° 52' 30"
12000N-
11000N-
10000N-
9000N-
8000N-
7000N-
6000N-
5000N-
4000N-
3000N-
2000N-
1000N-
0-
7
8
10
18
15
19
23
30
26
35
6
5
3
2
7
11
18
17
15
14
DDH 1 A
DDH 1 B
3000 W
2000 W
1000 W
0
1000 E
2000 E
3000 E
N
ROOSEVELT HOT SPRINGS KGRA
FIRST SEPARATION RESISTIVITY
DIPOLE–DIPOLE ARRAY
CONTOURS: 1,2,3,5,10,···
0 1 2 3 4 5 10
HUNDREDS OF METERS
100 M DIPOLES

Figure 44

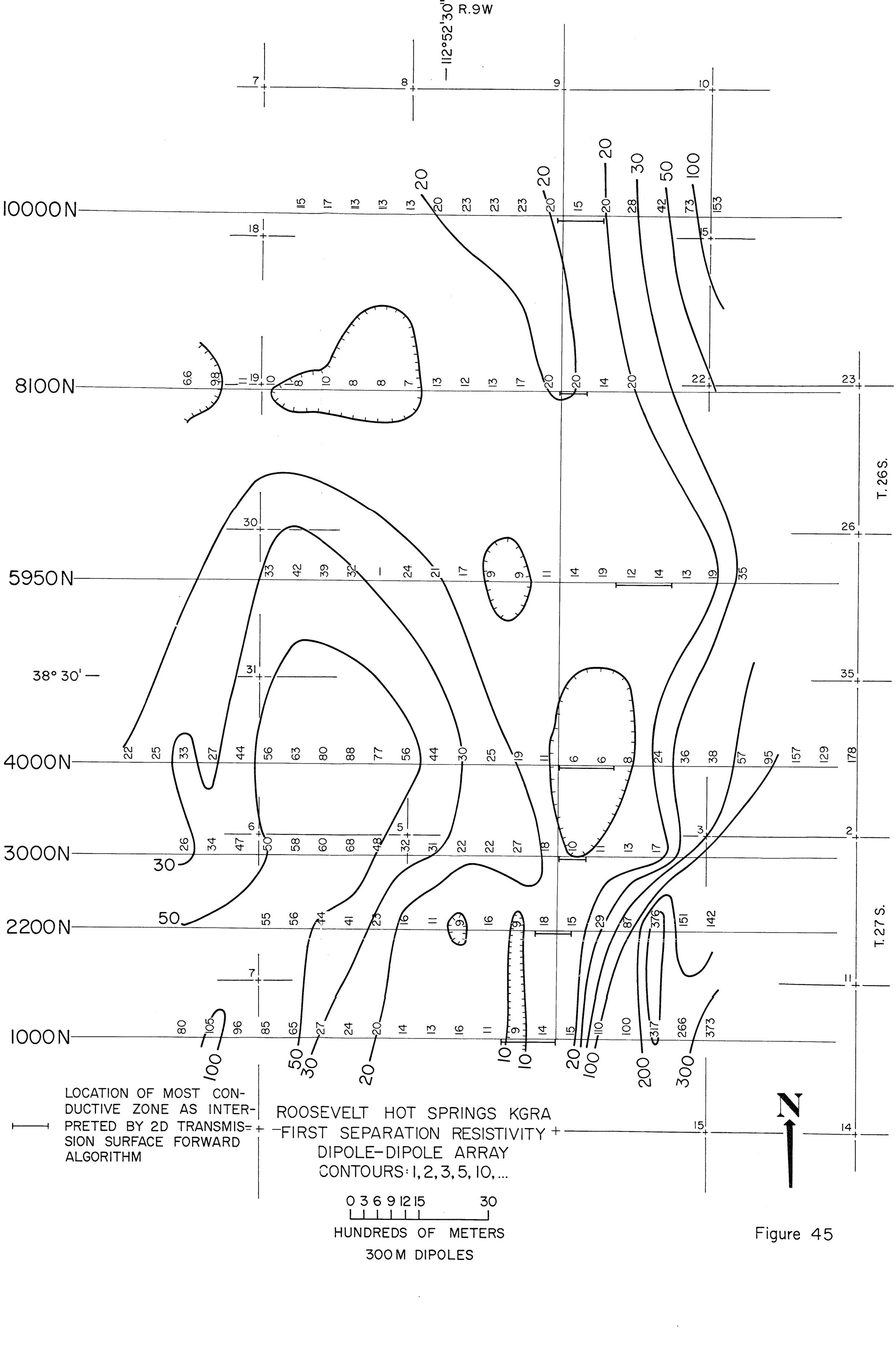
112°52'30"
R.9W
T. 26S.
T. 27 S.
38° 30'
10000N
8100N
5950N
4000N
3000N
2200N
1000N
LOCATION OF MOST CONDUCTIVE ZONE AS INTERPRETED BY 2D TRANSMISSION SURFACE FORWARD ALGORITHM
ROOSEVELT HOT SPRINGS KGRA
FIRST SEPARATION RESISTIVITY
DIPOLE-DIPOLE ARRAY
CONTOURS: 1, 2, 3, 5, 10, ...
0 3 6 9 12 15 30
HUNDREDS OF METERS
300 M DIPOLES
N

Figure 45

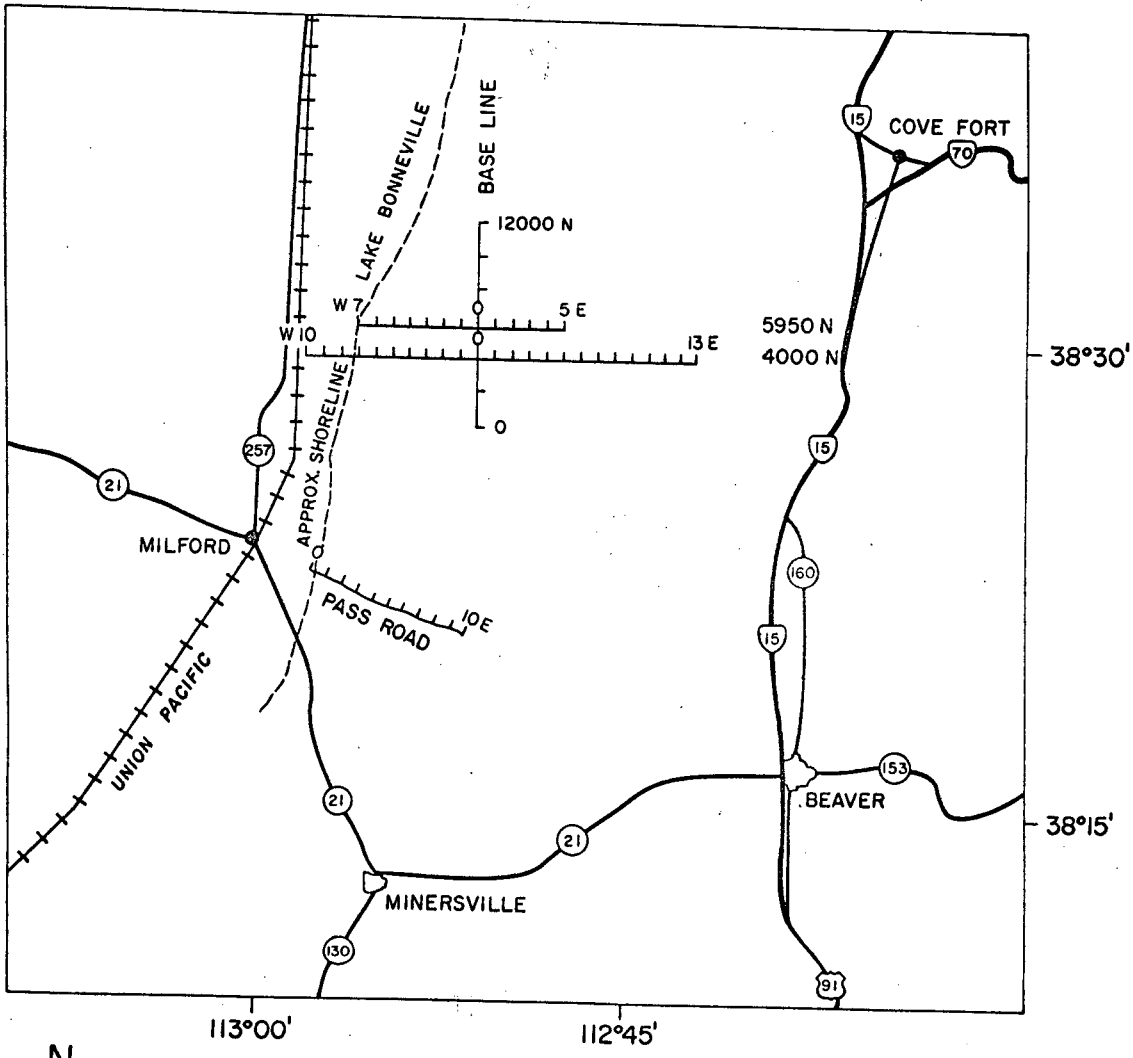
LAKE BONNEVILLE
BASE LINE
12000 N
W 7
5 E
W 10
13 E
0
APPROX. SHORELINE
COVE FORT
15
70
5950 N
4000 N
38°30'
257
21
MILFORD
PASS ROAD
10E
160
UNION PACIFIC
153
BEAVER
38°15'
MINERSVILLE
130
91
113°00'
112°45'
N
ROOSEVELT HOT SPRINGS KGRA
LOCATION OF TRAVERSE LINES
FOR 1 Km DIPOLE SURVEY
5 0 5 10 15 20 25 30
KILOMETERS

Figure 46

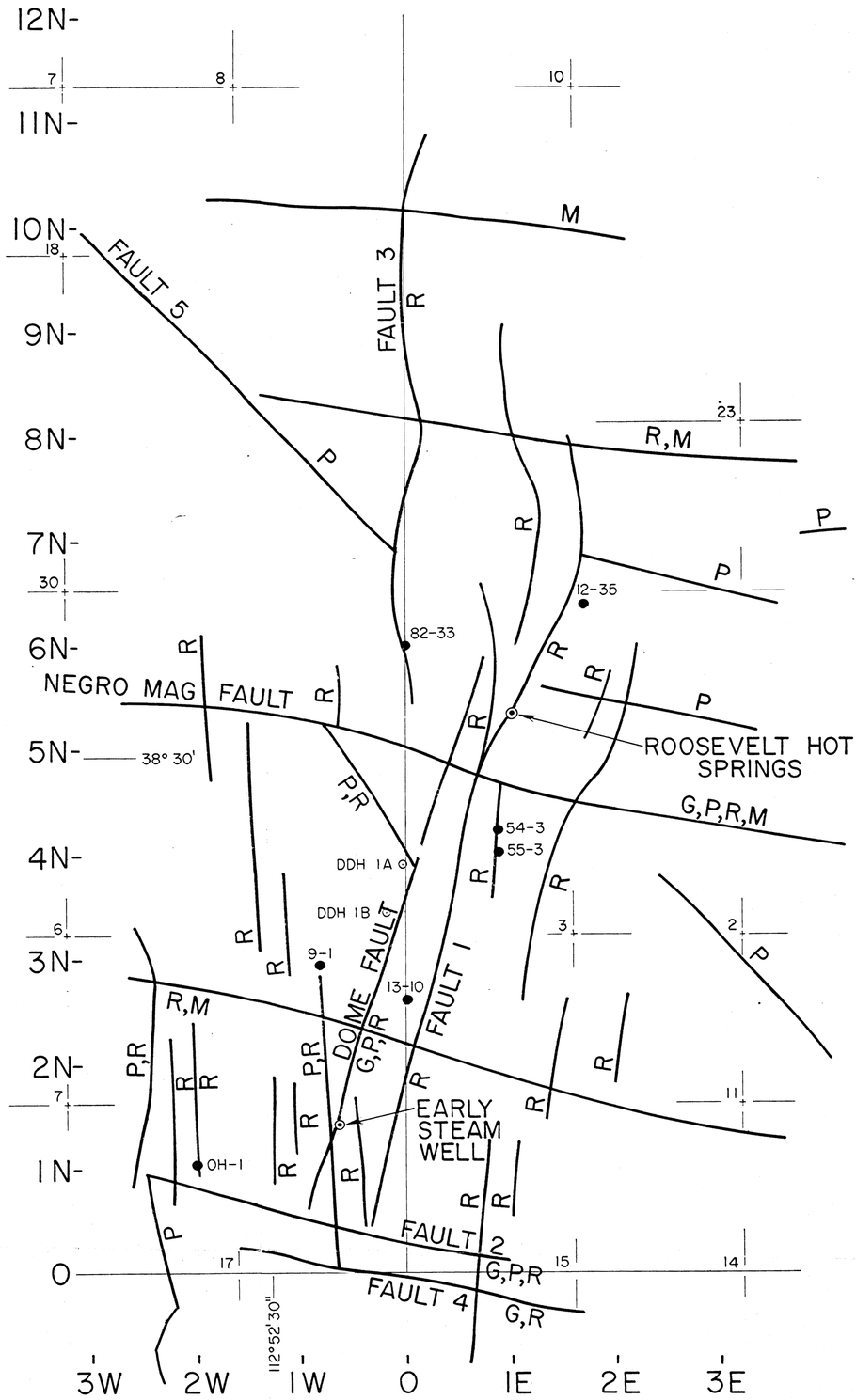

LEGEND

—— INTERPRETED FRACTURE

G,P,R,M,: GEOLOGY, PHOTO, RESISTIVITY, MAGNETICS

• WELL BY PHILLIPS PETROLEUM CO.

○ DDH BY U OF U

N

ROOSEVELT HOT SPRINGS KGRA
INTERPRETED FRACTURES

SCALE 0 .5 1.0
KILOMETERS

Figure 47

RESISTIVITIES (Ω-m)		THICKNESSES (m)	
ρ_1 =	132 ± 4.4%	t_1 =	4.31 ± 7.4%
ρ_2 =	31.7 ± 6.2%	t_2 =	30.5 ± 13.0%
ρ_3 =	10.8 ± 11.4%	t_3 =	145 ± 12.4%
ρ_4 =	88000 ± 12.4%		

SCHLUMBERGER VES INVERSE SOLUTION
ROOSEVELT HOT SPRINGS KGRA
LOCATION 100 W × 3500 N

Figure 48

LINE 1000 N.

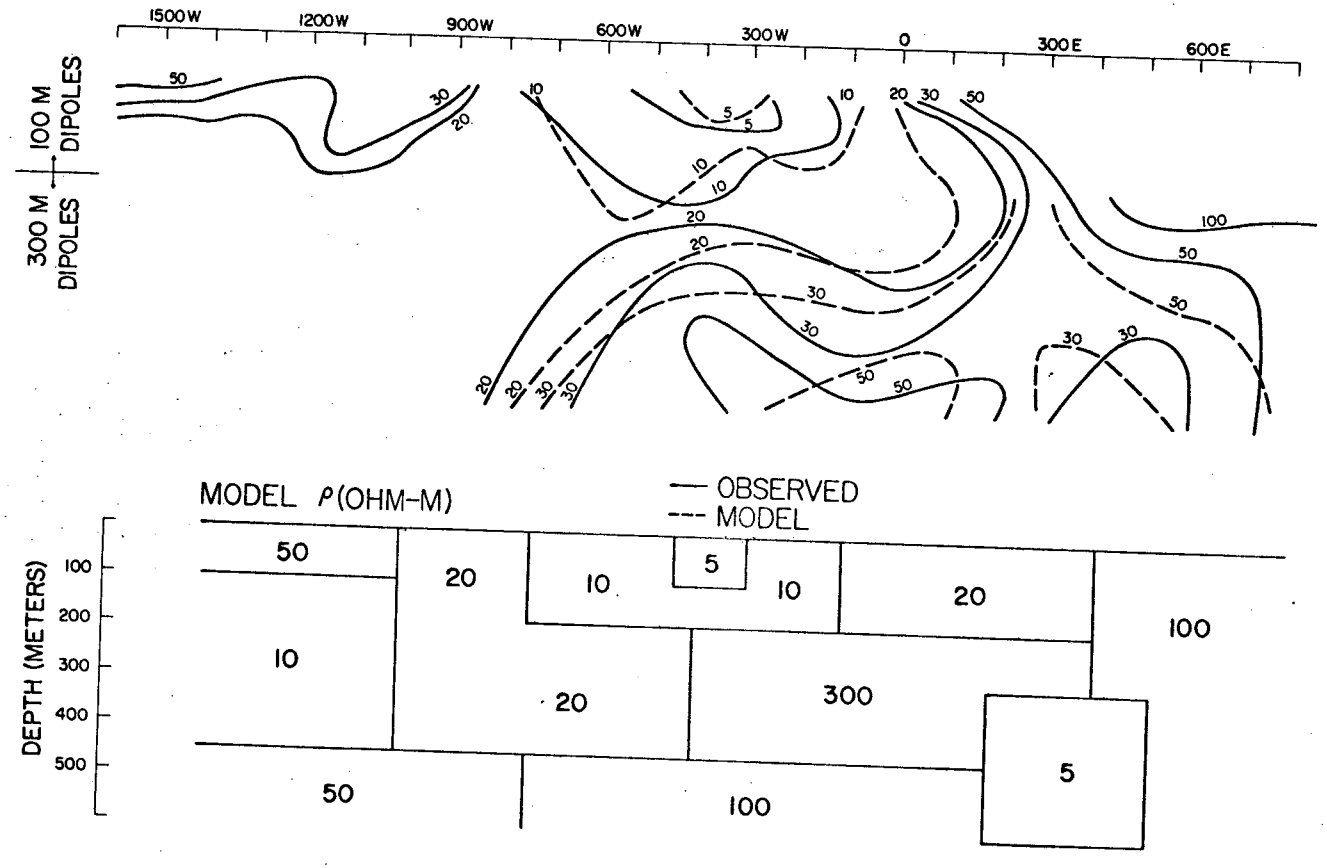

ROOSEVELT HOT SPRINGS KGRA
OBSERVED & INTERPRETED RESISTIVITY

SCALE
0 300 600
METERS

Figure 49

LINE 3000N.

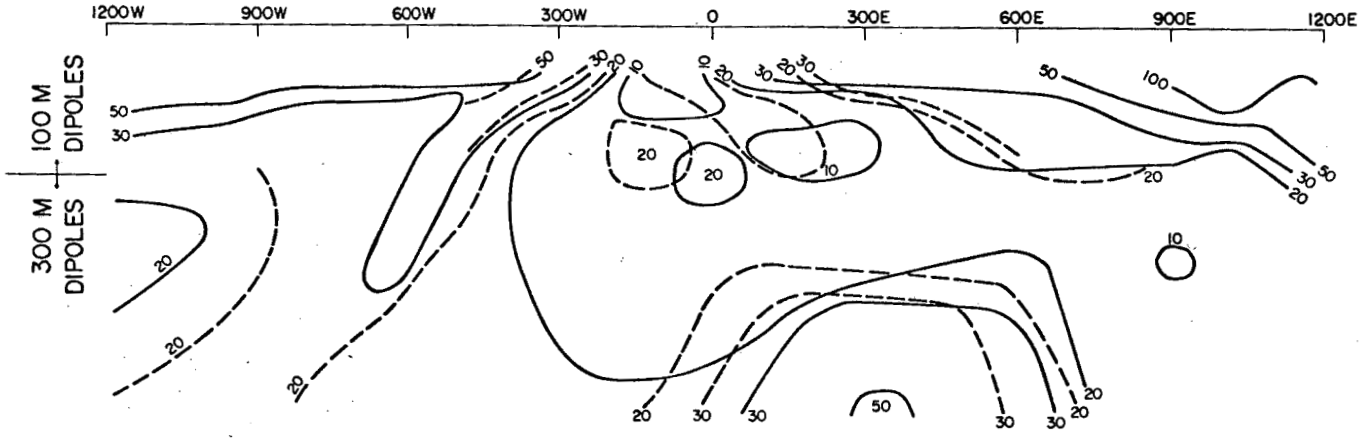

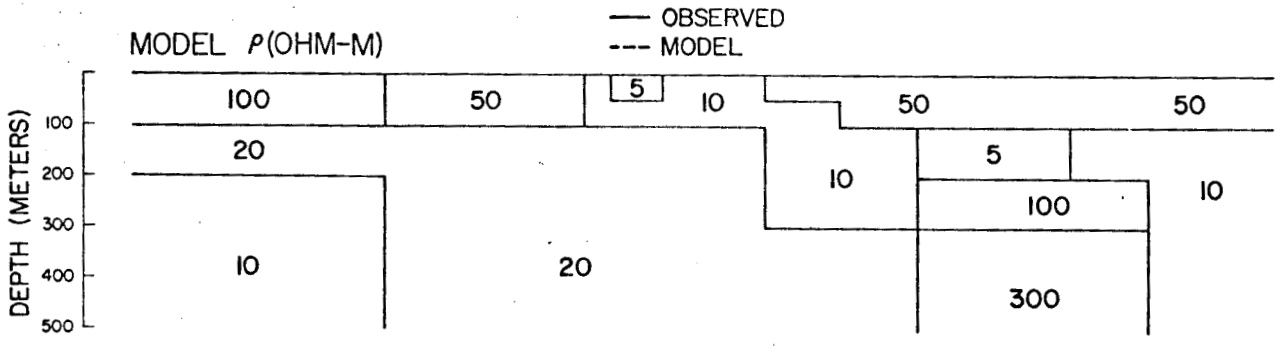

ROOSEVELT HOT SPRINGS KGRA
OBSERVED & INTERPRETED RESISTIVITY

SCALE
0 300 600
METERS

Figure 50

LINE 4000 N.

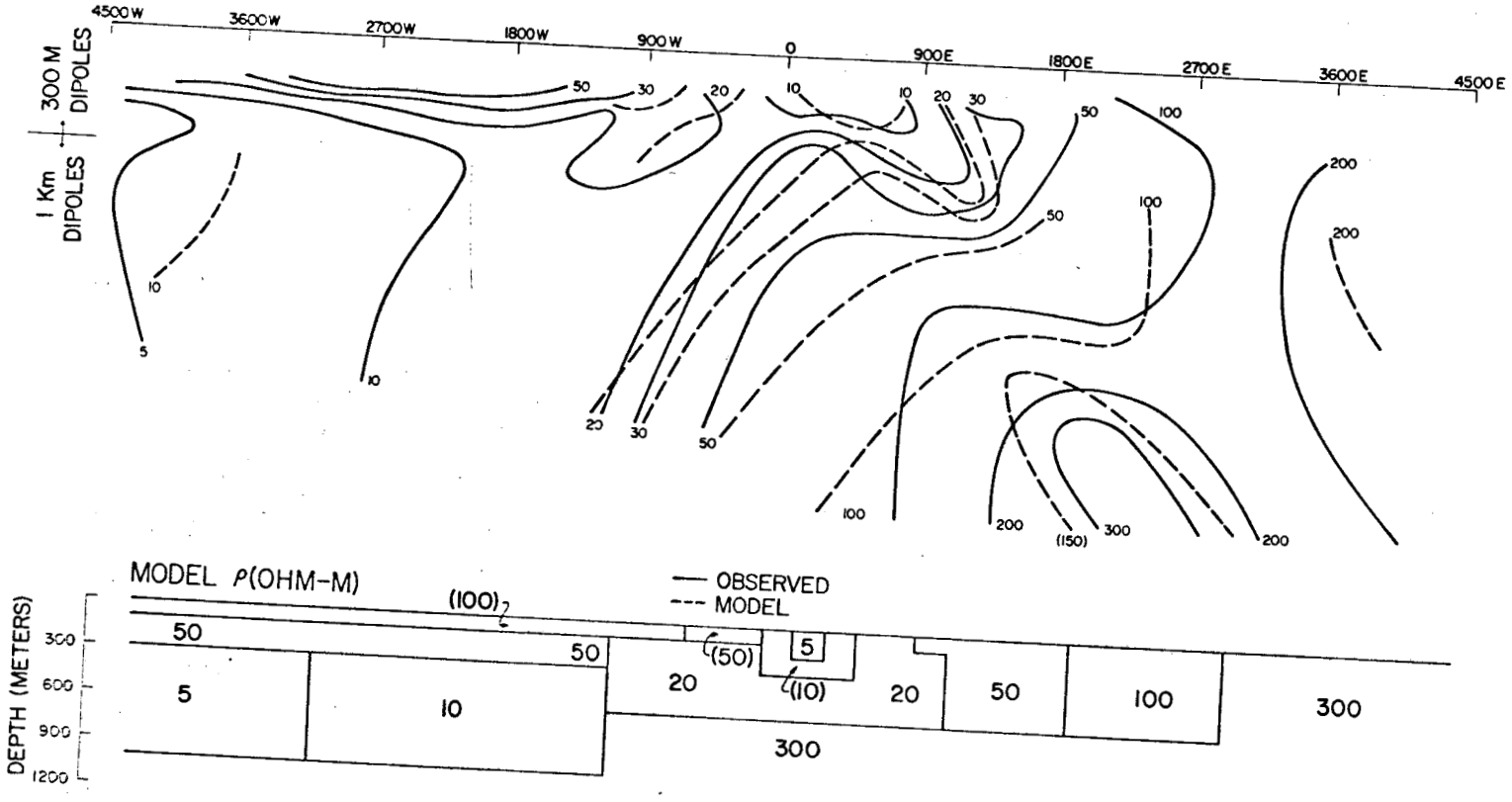

ROOSEVELT HOT SPRINGS KGRA
OBSERVED & INTERPRETED RESISTIVITY

SCALE
0 500 1000
METERS

Figure 51

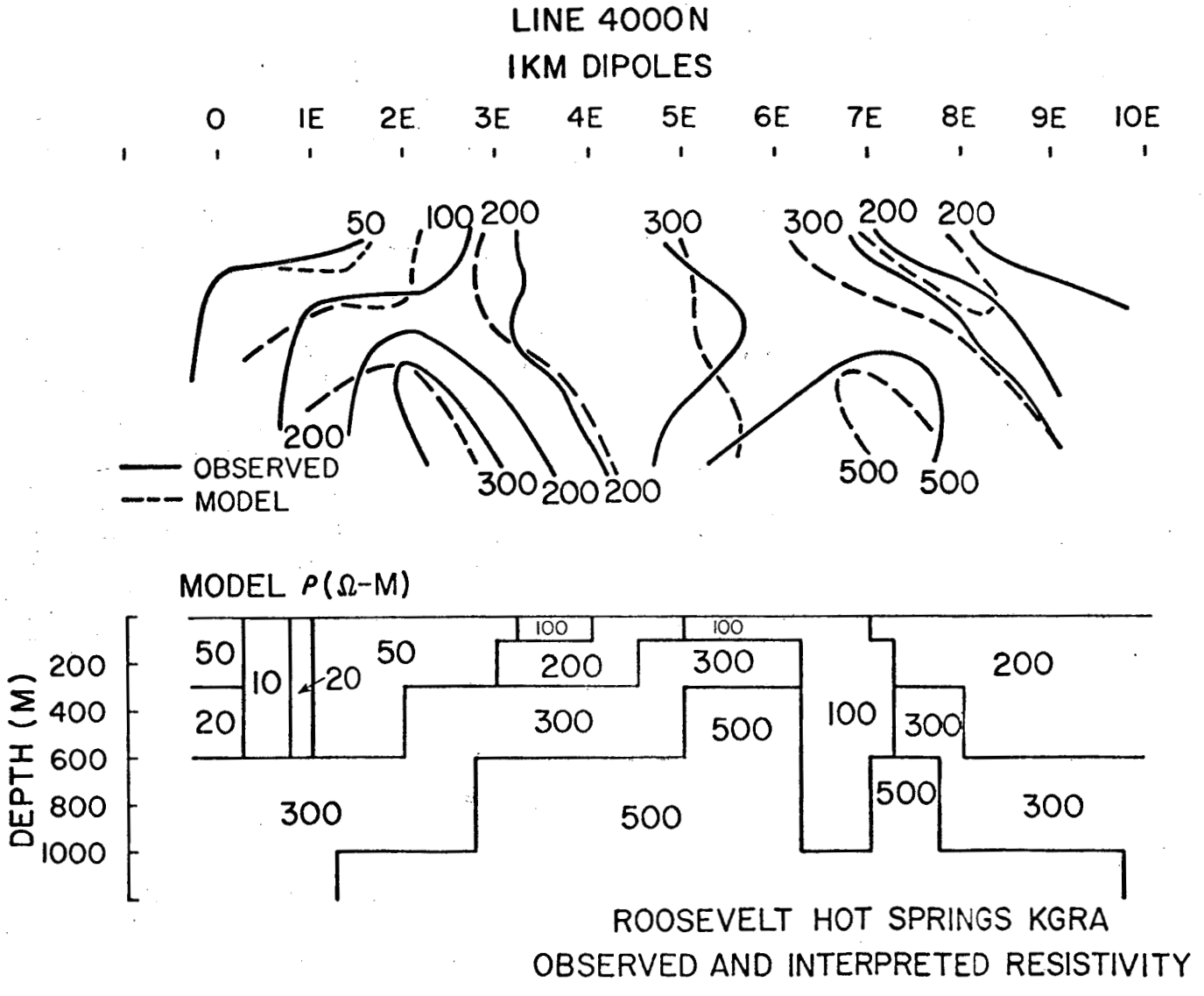
LINE 4000N
1KM DIPOLES
0
1E
2E
3E
4E
5E
6E
7E
8E
9E
10E
50
100
200
300
300
200
200
200
300
200
200
500
500
OBSERVED
MODEL
MODEL P(Ω-M)
DEPTH (M)
200
400
600
800
1000
50
10
20
50
100
100
200
300
200
20
300
500
100
300
500
300
500
300
ROOSEVELT HOT SPRINGS KGRA
OBSERVED AND INTERPRETED RESISTIVITY

Figure 52

LINE 8100N.

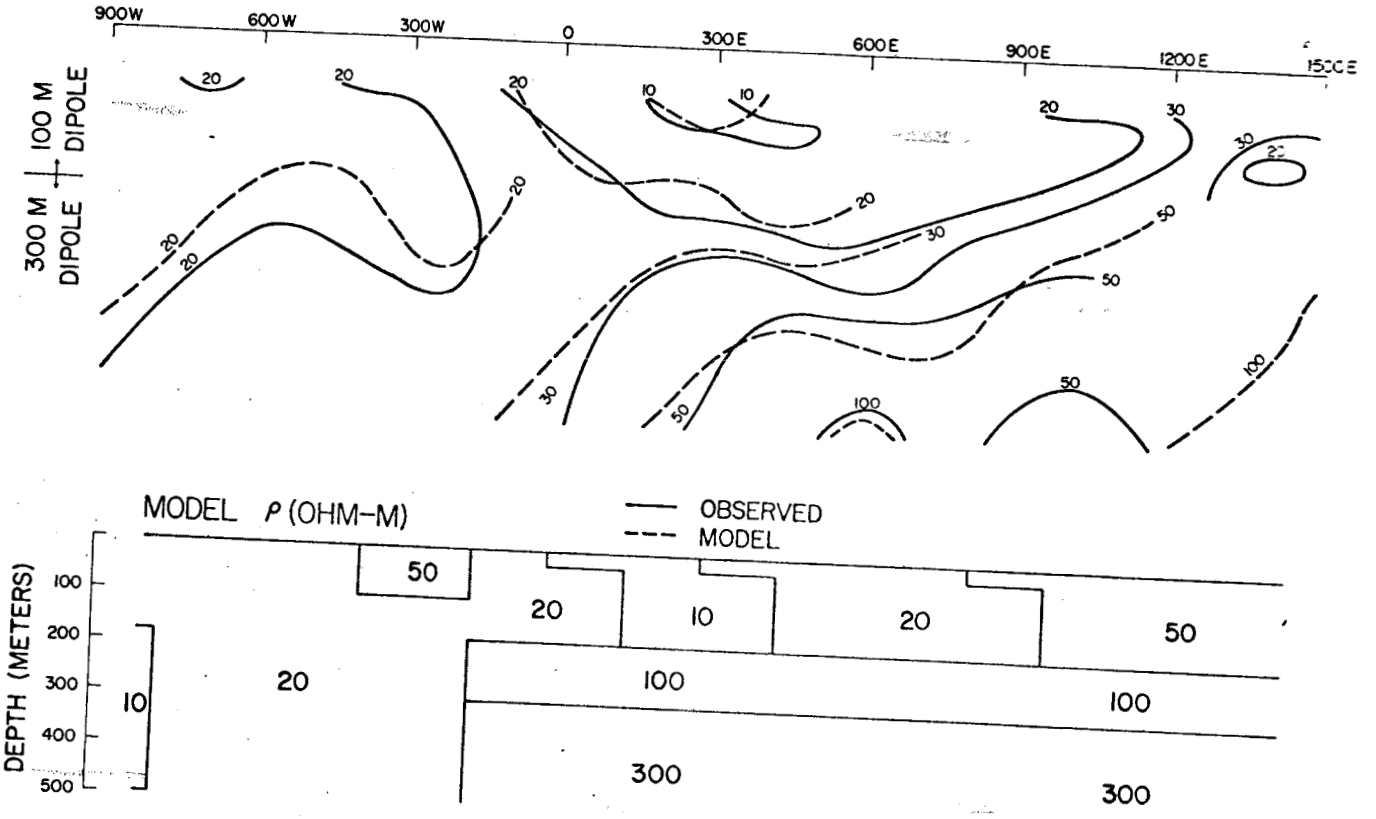

ROOSEVELT HOT SPRINGS KGRA
OBSERVED & INTERPRETED RESISTIVITY

SCALE
0 300 600
METERS

Figure 53

LINE 4000N 1KM DIPOLES

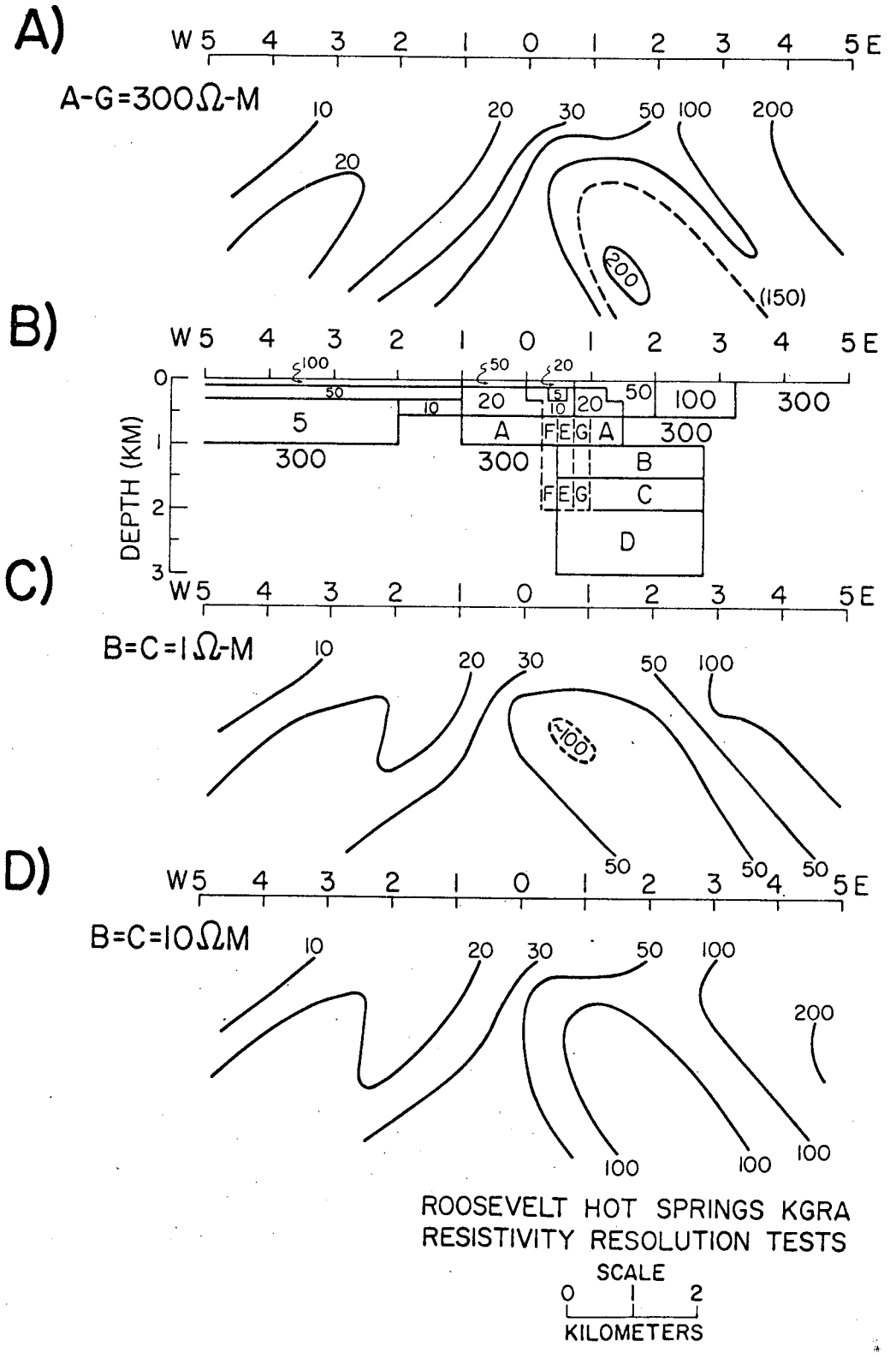

ROOSEVELT HOT SPRINGS KGRA
RESISTIVITY RESOLUTION TESTS

SCALE
0 1 2
KILOMETERS

Figure 54

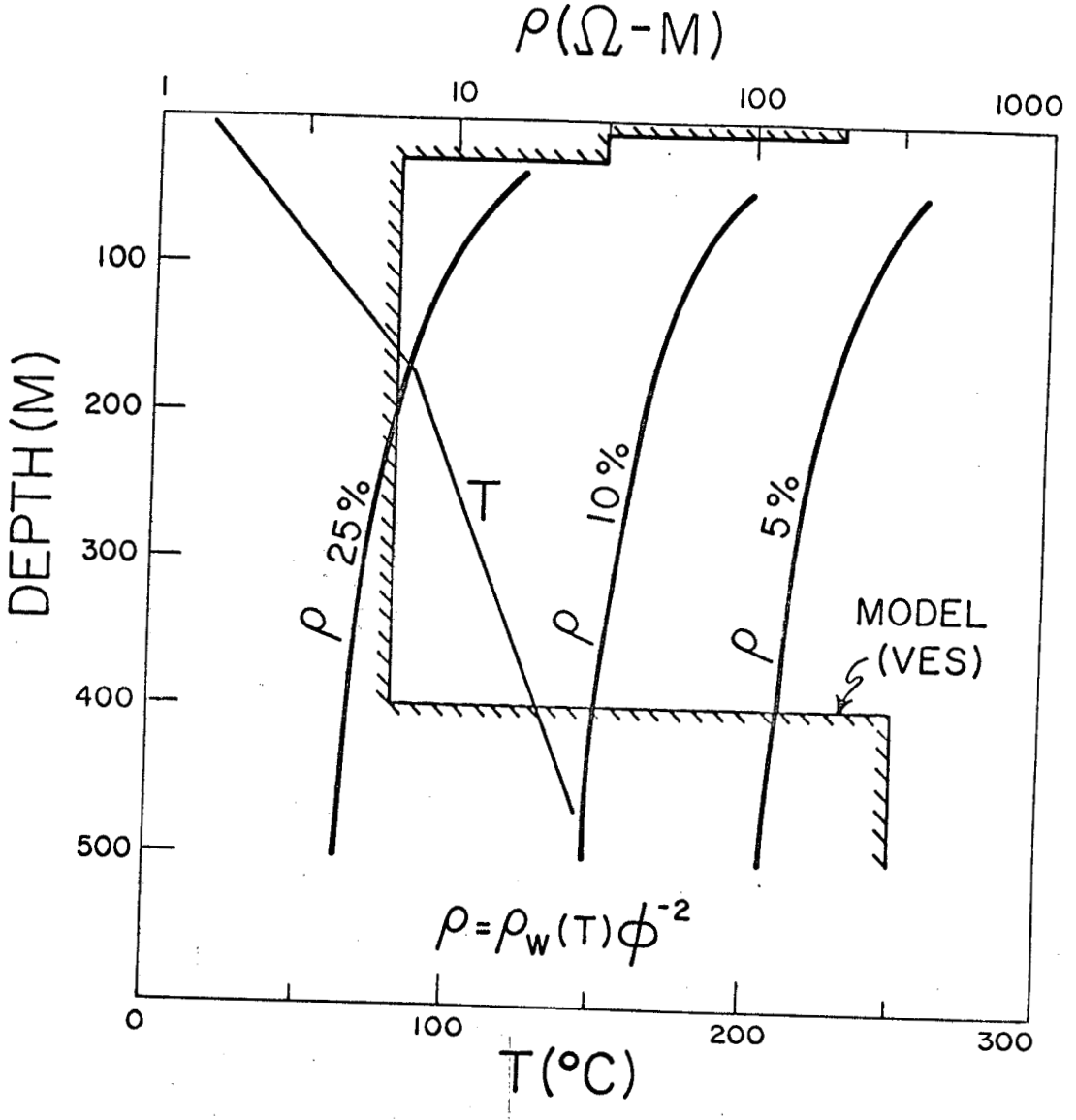
ρ(Ω-M)
1
10
100
1000
DEPTH (M)
100
200
300
400
500
ρ 25%
T
ρ 10%
ρ 5%
MODEL
(VES)
ρ=ρw(T)φ^-2
0
100
200
300
T(°C)

Figure 55